Active Galactic Nuclei

NGC 1068 (M77)
(Nordic Optical Telescope)

Introduction

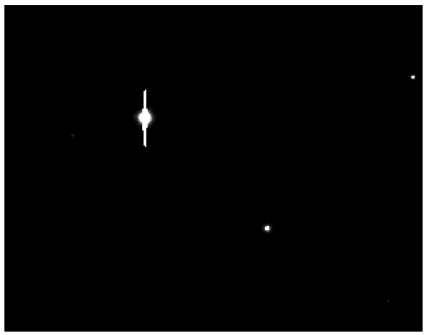

NGC 3783: *linear* intensity scale

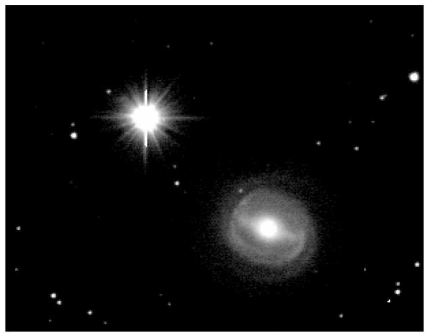

logarithmic intensity scale

Active Galactic Nuclei (AGN): Galaxies with centers as bright as a whole galaxy

1908: E. Fath

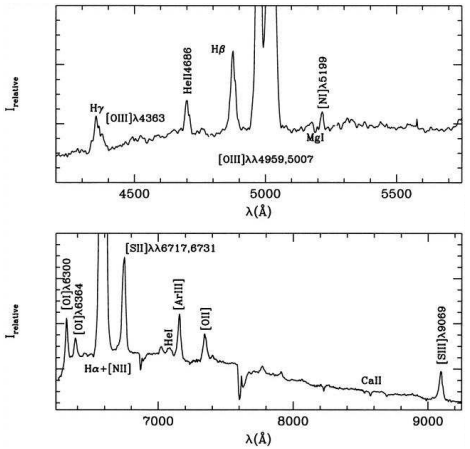

Optical spectrum of NGC 1068

(García-Lorenzo et al., 1999, Fig. 4)

1908: Edward A. Fath: Emission lines in NGC 1068 are similar to those seen in planetary nebulae.

Part of his dissertation!

Differences: very high degree of ionization, large line widths

1918: H. Curtis

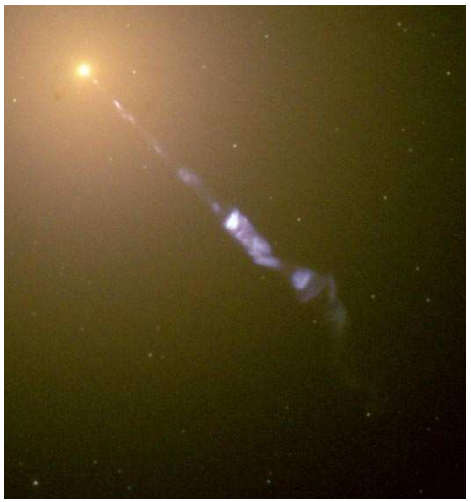

HST

1918: Heber D. Curtis: “[M87 exhibits] a curious straight ray. . . apparently connected with the nucleus by a thin line of matter”.

$\Longrightarrow$ M87 contains an optical jet

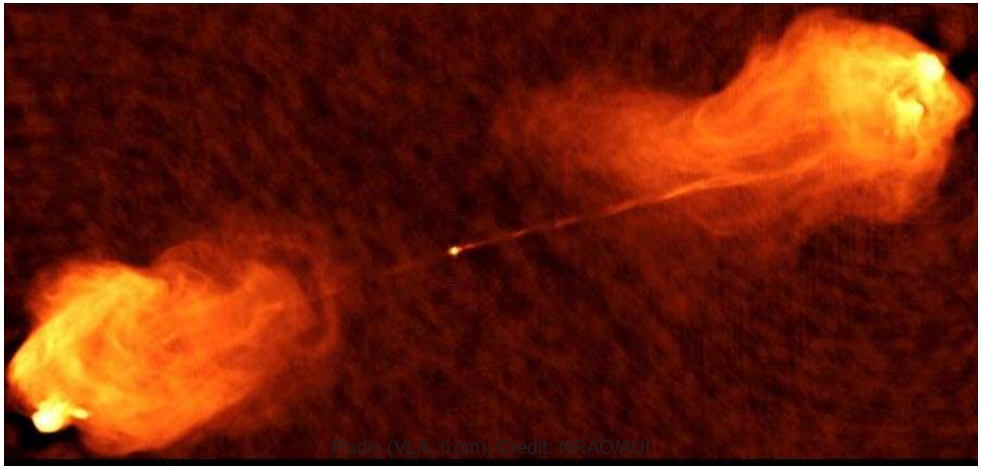

The powerful radio galaxy Cygnus A

1943: C. Seyfert

NUCLEAR EMISSION IN SPIRAL NEBULAE*

Carl K. Seyfert†

ABSTRACT

Spectrograms of dispersion 37–200 A/mm have been obtained of six extragalactic nebulae with high-excitation nuclear emission lines superposed on a normal G-type spectrum. All the stronger emission lines from λ 3727 to λ 6731 found in planetaries like NGC 7027 appear in the spectra of the two brightest spirals observed, NGC 1068 and NGC 4151.

Apparent relative intensities of the emission lines in the six spirals were reduced to true relative intensities. Color temperatures of the continua of each spiral were determined for this purpose.

The observed relative intensities of the emission lines exhibit large variations from nebula to nebula. Profiles of the emission lines show that all the lines are broadened, presumably by Doppler motion, by amounts varying up to 8500 km/sec for the total width of the hydrogen lines in NGC 3516 and NGC 7469. The hydrogen lines in NGC 4151 have relatively narrow cores with wide wings, 7500 km/sec in total breadth. Similar wings are found for the Balmer lines in NGC 7469. The lines of the other ions show no evidence of wide wings. Some of the lines exhibit strong asymmetries, usually in the sense that the violet side of the line is stronger than the red.

In NGC 7469 the absorption K line of *Ca* II is shallow and 50 A wide, at least twice as wide as in normal spirals.

Absorption minima are found in six of the stronger emission lines in NGC 1068, in one line in NGC 4151, and one in NGC 7469. Evidence from measures of wave length and equivalent widths suggests that these absorption minima arise from the G-type spectra on which the emissions are superposed.

The maximum width of the Balmer emission lines seems to increase with the absolute magnitude of the nucleus and with the ratio of the light in the nucleus to the total light of the nebula. The emission lines in the brightest diffuse nebulae in other extragalactic objects do not appear to have wide emission lines similar to those found in the nuclei of emission spirals.

(Seyfert, 1943)

1943: Carl Seyfert: There is a class of spiral galaxies with optical *emission lines*

$\Longrightarrow$ Seyfert Galaxies

1954: W. Baade and R. Minkowski

W. Baade (Mt. Wilson Obs.)

IDENTIFICATION OF THE RADIO SOURCES IN CASSIOPEIA, CYGNUS A, AND PUPPIS A

W. Baade and R. Minkowski
Mount Wilson and Palomar Observatories
Carnegie Institution of Washington
California Institute of Technology

Received June 19, 1953

ABSTRACT

The radio sources in Cassiopeia and Puppis A are identified with a new type of galactic emission nebulosity. The outstanding features of these nebulosities are very large internal random velocities. The radio source Cygnus A is an extragalactic object, two galaxies in actual collision.

Only very few individual sources of cosmic radio emission have been identified with conspicuous astronomical objects.[1] Although the sources in Cassiopeia[2] and Cygnus A[3]

(Baade & Minkowski, 1954)

1954: Walter Baade and Rudolph Minkowski: Bright radio sources have galaxies as optical counterparts

Cyg A: 2nd brightest extrasolar radio source on the sky.

1959: L. Woltjer

EMISSION NUCLEI IN GALAXIES

L. WOLTJER*
Yerkes Observatory, University of Chicago
Received February 16, 1959

ABSTRACT

Some galaxies which show wide emission lines in the spectra of their nuclei are discussed. It is shown that, on statistical grounds, the nuclear emission must last for several times 10^8 years at least. The nuclei are extremely narrow, of the order of 100 parsecs, and, if a normal mass-to-light ratio applies, extremely massive. The width of the emission lines, which indicates velocities of a few thousand kilometers per second, is probably due to fast motions, circular or random, in the gravitational fields of the nuclei. The high star density in the nuclei may provide a source of excitation. In the nucleus of our own Galaxy the radio source Sagittarius gives evidence of strong magnetic fields and large amounts of relativistic particles. A mass of a few times 10^8 solar masses is needed to prevent disintegration of the source. The Andromeda Nebula has a nucleus with a somewhat smaller mass. The occurrence of dense nuclei may be a common characteristic of many galaxies.

(Woltjer, 1959)

1959: Lodewijk Woltjer: Objects must have very large masses.

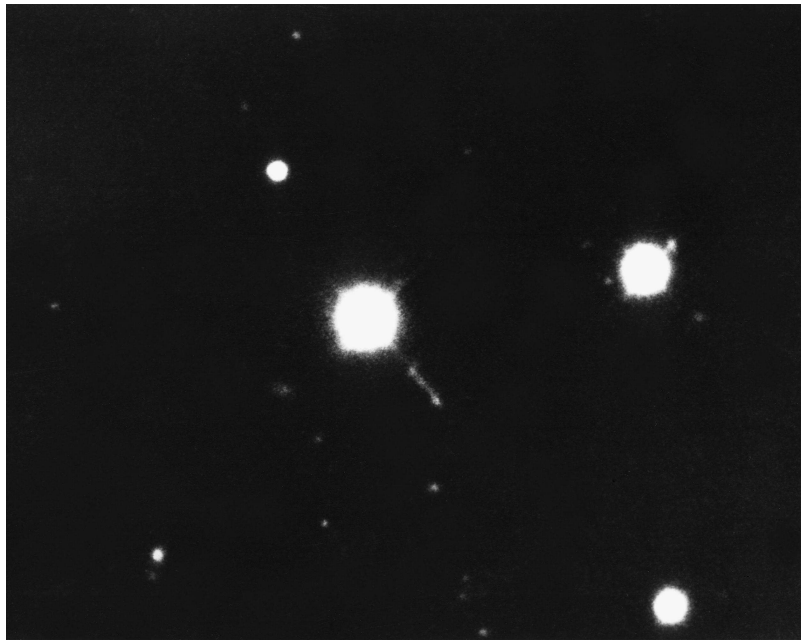

3C273 (4 m Myall telescope, NOAO/AURA/NSF)

1963: M. Schmidt

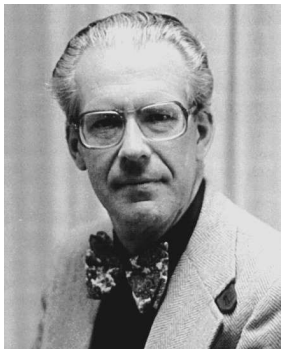

M. Schmidt (Caltech)

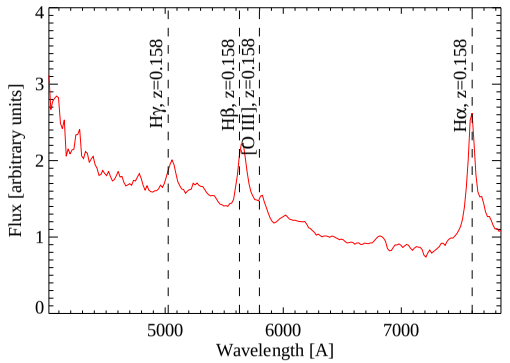

3C273 (Rondi et al., Pic du Midi)

1963: Maarten Schmidt: 3C273 has $z = 0.158 \Longrightarrow$ objects are far away!

$z = 0.158$ corresponds to $d = 0.7$ Gpc (2 billion ly)

shortly after this: 1963: J. Greenstein and Th. Matthews: 3C48 has $z = 0.368$

Seyfert Galaxies

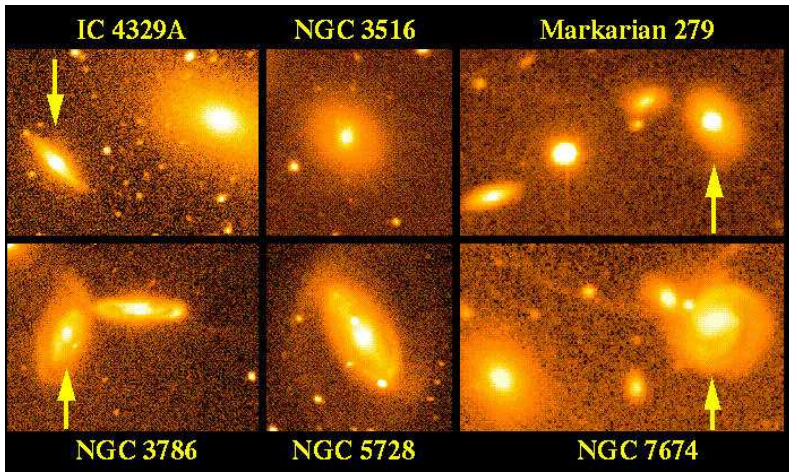

W. Keel

Seyfert Galaxies: point-like sources in the centers of galaxies, normally galaxy is detectable; two types: Seyfert 1 galaxies and Seyfert 2 galaxies.

Seyfert Galaxies

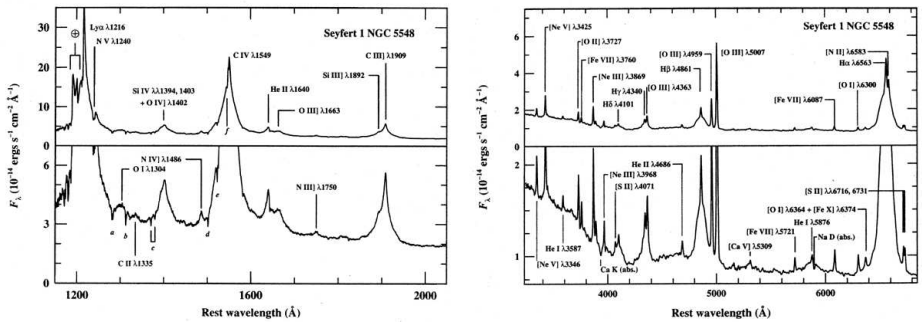

Seyfert 1 galaxies

- broad allowed lines (e.g., from H), with widths corresponding up to $10^4\,\mathrm{km\,s^{-1}}$ from a medium of high density ($n_\mathrm{e} \gtrsim 10^9\,\mathrm{cm^{-3}}$).
- Thin forbidden lines (e.g., [O III]5007), FWHM $\sim$ few $\cdot\, 10^2\,\mathrm{km\,s^{-1}}$ from a thin medium ($n_\mathrm{e} \sim 10^3\,\mathrm{cm^{-3}} \ldots 10^6\,\mathrm{cm^{-3}}$).

Velocity width from Doppler effect: $\Delta\lambda/\lambda = v/c$.

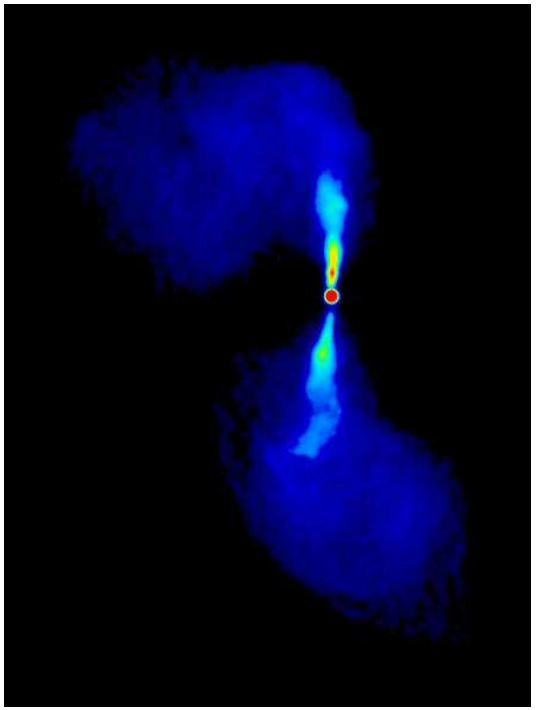

Radio image of M84 (3C272.1):
A typical Fanaroff Riley Type 1 Galaxy

Laing & Bridle (1987); VLA 4885 MHz, $134'' \times 170''$

Seyfert 2

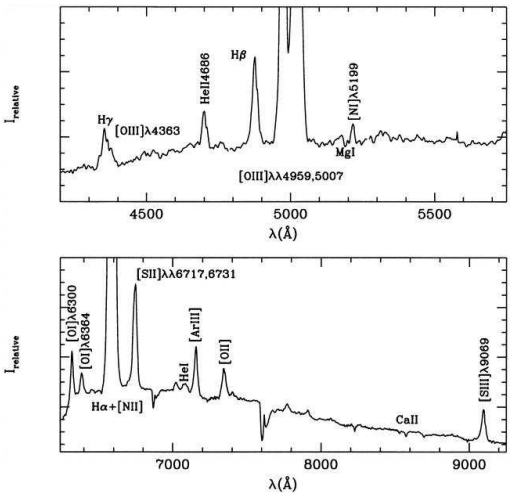

Spectrum of the Seyfert 2 galaxy NGC 1068:

- weak continuum (compared to Seyfert 1s).
- thin forbidden lines, $\sim$ few $\cdot\, 10^2\,\mathrm{km\,s^{-1}}$.
- no broad lines

(García-Lorenzo et al., 1999, Fig. 4)

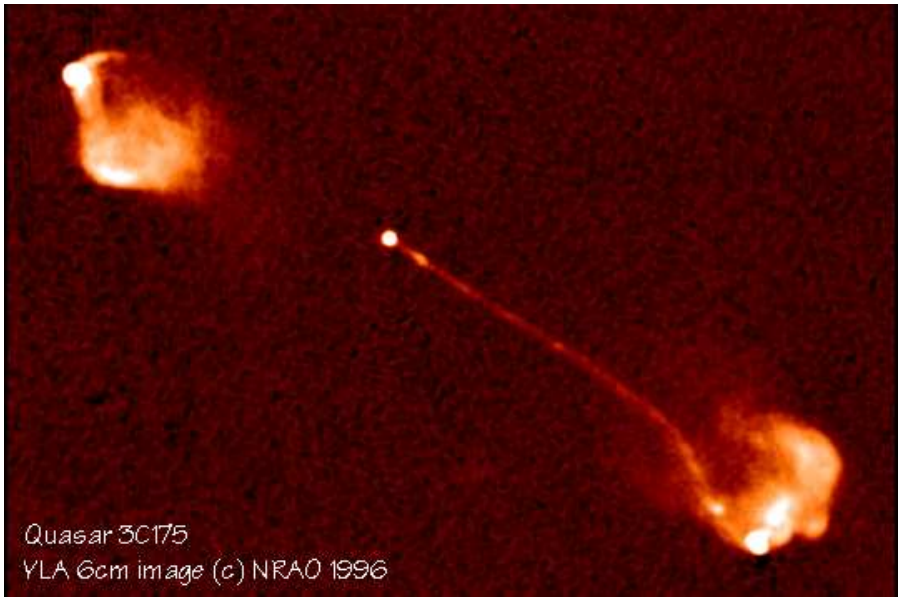

A. Bridle (priv. comm.)

Radio image of 3C175 ($z = 0.768$):
A typical FR 2 Galaxy

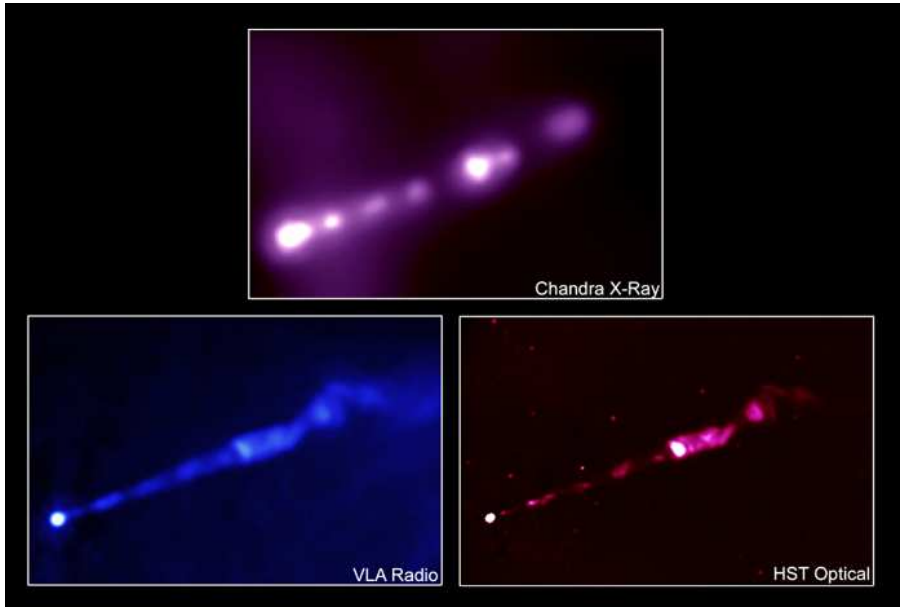

X-ray: NASA/CXC/MIT/H.Marshall et al. Radio: F.Zhou, F.Owen (NRAO), J.Biretta (STScI)
Optical: NASA/STScI/UMBC/E.Perlman et al.

Since the 1960s: multi wavelength astronomy

M87 – R. Gendler

http://www.robgendlerastropics.com/M87NM.html

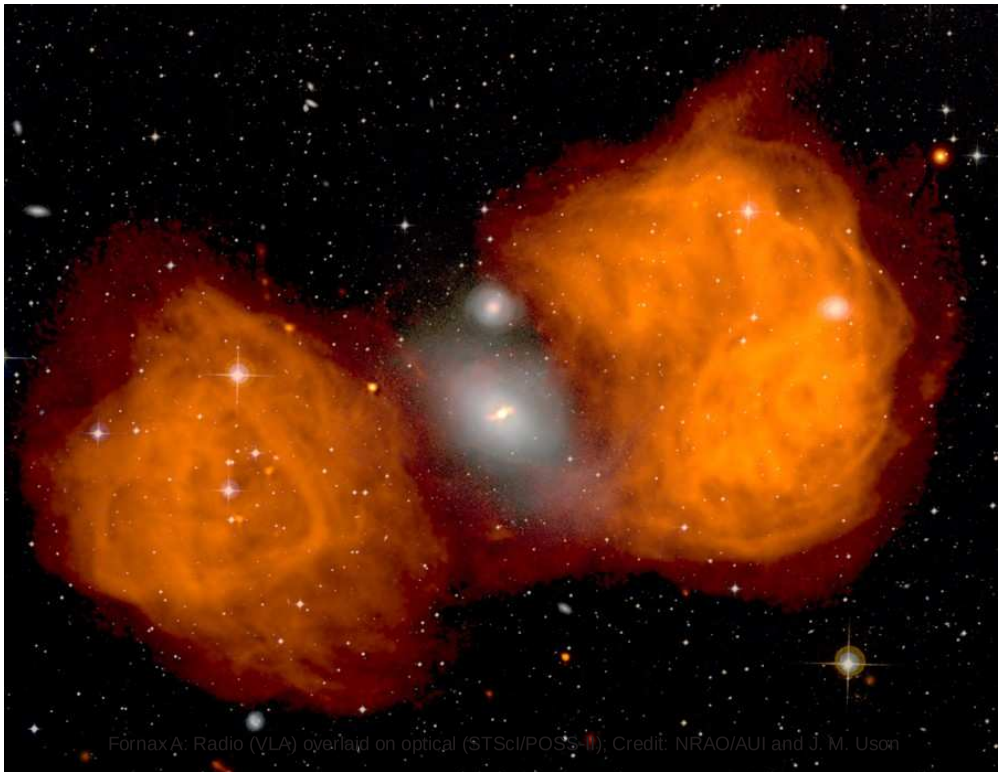

Fornax A: Radio (VLA) overlaid on optical (STScI/POSS-II). Credit: NRAO/AUI and J. M. Uson

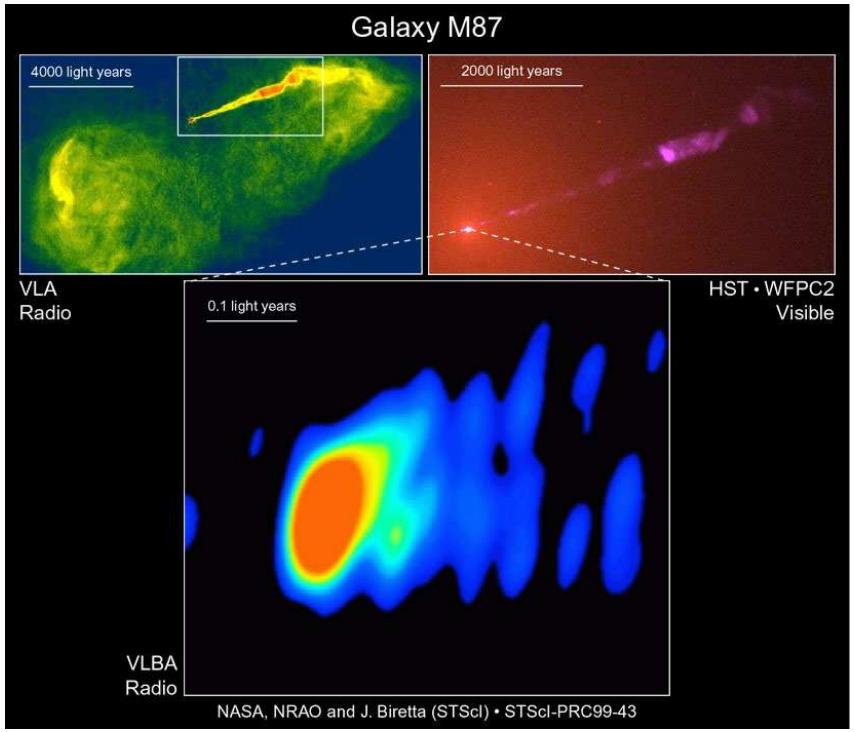

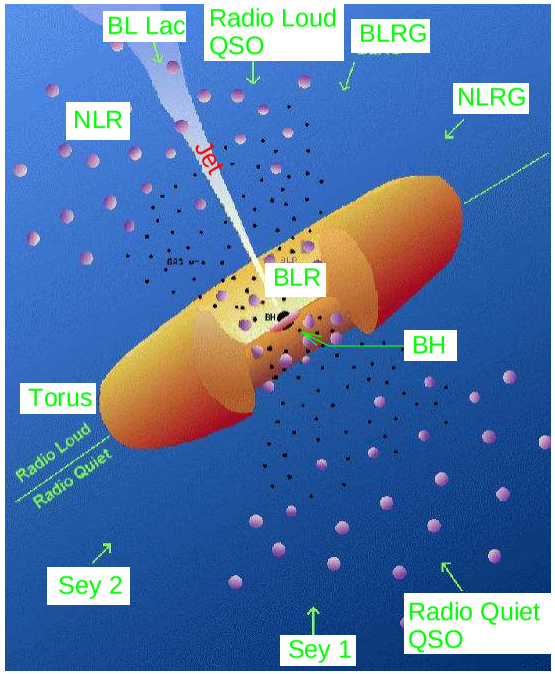

Unification: Assumes physics of all AGN is the same, phenomenology is due to different lines of sight.

(Urry & Padovani, 1995, Important: length scale is not linear!)

X-Ray Spectra

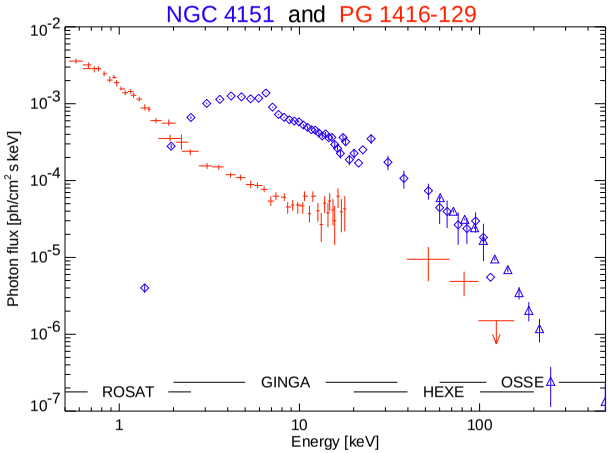

(PG 1416−129: de Kool et al., 1994, Williams et al., 1992, Staubert & Maisack, 1996; NGC 4151: Maisack 1991, 1993)

Note: NGC 4151 not corrected for interstellar absorption.

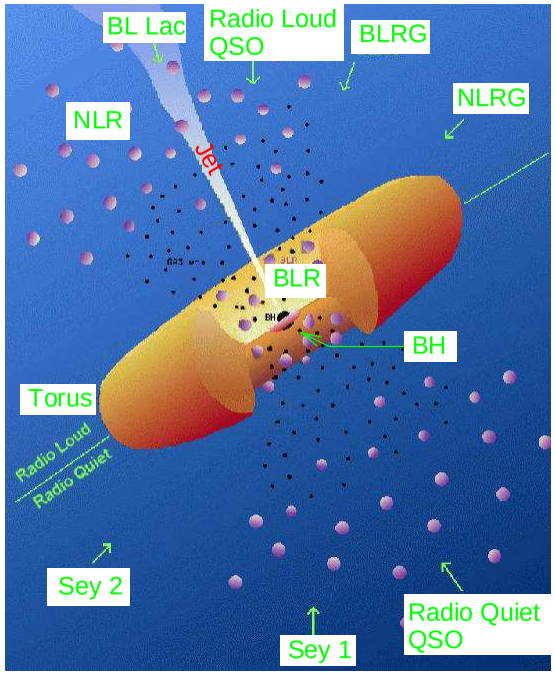

Physical properties:

Accretion disc: $r \sim 10^{-3}$ pc,
$n \sim 10^{15}$ cm^{-3},
$kT \sim 50\,\mathrm{eV} \cdot r^{-3/4}$,
$v \sim 0.3c$ at the inner edge.

Broad Line Region (BLR): $r \sim$ 0.01–0.1 pc (=light days or less),
$n \sim 10^{10}$ cm^{-3},
$v \sim$ 1000–5000 km s^{-1},
$T \sim 10^4$ K

Torus: $r \sim$ 1– few 10 pc,
$n \sim 10^3$–10^6 cm^{-3},
T: cold

Narrow Line Region (NLR):
$r \sim$ 100–1000 pc,
$n \sim 10^3$–10^6 cm^{-3},
$v \sim$ few100 km s^{-1},
$T \sim 10^4$ K

X-Ray Spectra

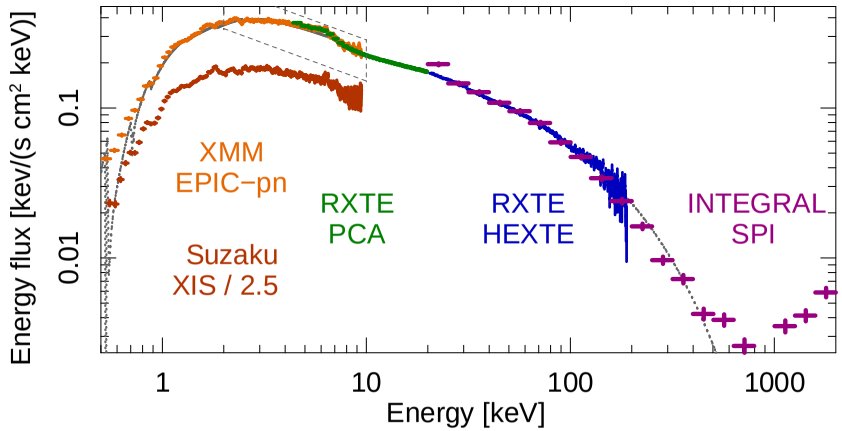

Cyg X-1 (Hanke, et al., 2008)

Spectral shape of Seyferts is very similar to Galactic Black Holes ⟹
Same physical mechanism (=Comptonization) responsible!

Comptonization

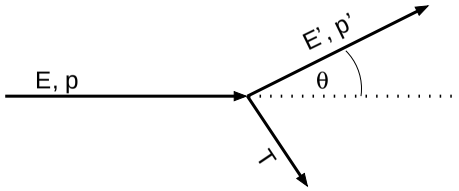

Thomson scattering: initial and final wavelength are identical.
Photon picture:
$\Longrightarrow$ Scattering: photon changes direction
$\Longrightarrow$ Momentum change
$\Longrightarrow$ Energy change!
$\Longrightarrow$ Compton scattering.

Dynamics of scattering gives energy/wavelength change:

$$E' = \frac{E}{1 + \frac{E}{m_e c^2}(1 - \cos\theta)} \quad \text{or} \quad \lambda' - \lambda = \frac{h}{m_e c}(1 - \cos\theta) \tag{9.1}$$

Averaging over θ, for $E \ll m_e c^2$:

$$\frac{\Delta E}{E} \approx -\frac{E}{m_e c^2} \tag{9.2}$$

For thermal photons: energy transfer onto electron possible:

$$\frac{\Delta E}{E} = \frac{4kT - E}{m_e c^2} \tag{9.3}$$

Simple Reflection

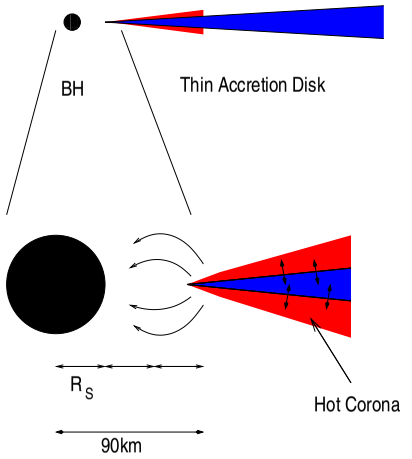

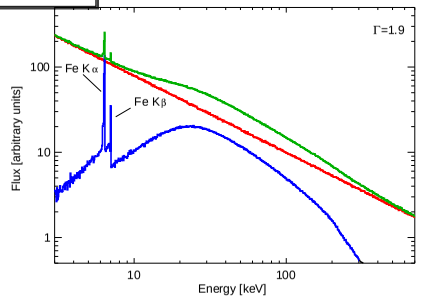

XRB/AGN X-Ray Spectrum:

- Comptonization of soft X-rays from accretion disk in hot corona ($T \sim 10^8$ K): power law continuum.
- Thomson scattering of power law photons in disk: Compton Reflection Hump
- Photoabsorption of power law photons in disk: fluorescent Fe Kα Line at ∼6.4 keV

Models: Guilbert & Rees (1988), Lightman & White (1988), Magdziarz & Zdziarski (1995), Ross & Fabian (2007). Reviews: Turner & Miller (2009), Fabian & Ross (2010).

Comptonization

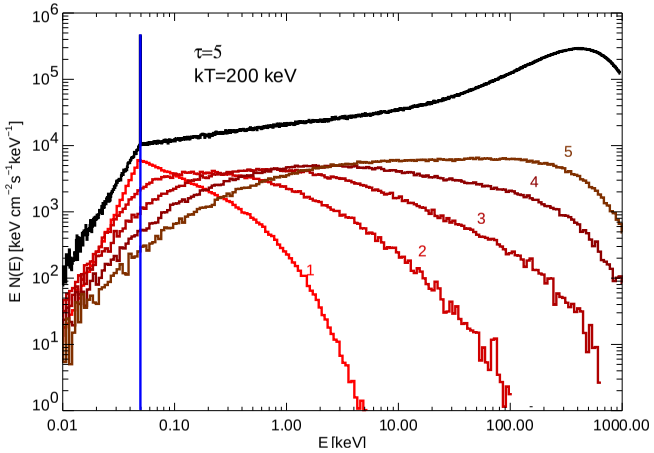

Monte Carlo simulation shows: Spectrum is $\Longrightarrow$ Power law with exponential cut-off (here: with additional “Wien hump”).

Seyfert X-Ray Spectra

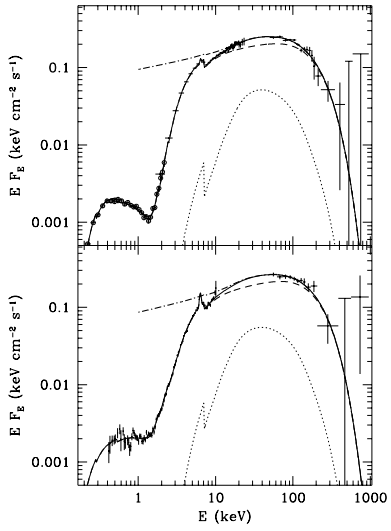

Comptonization explains broad-band Seyfert spectra very well

Example: Fits of Comptonization models to broad-band spectrum of Seyfert 1 galaxy NGC 4151 showing all three components:

- $kT_e \sim 88^{+55}_{-26}$ keV
- $N_H \sim 7 \times 10^{22}$ cm^{-2} and 13×10^{22} cm^{-2}, respectively
- Reflection factor: $\Omega/2\pi = 0.43$ (assumed; consistent with Fe line, but not significantly detected in these data [but in other AGN]).

Note strong absorption present in Seyfert 1 X-ray spectra!

(Zdziarski et al., 1996)

Seyfert X-Ray Spectra

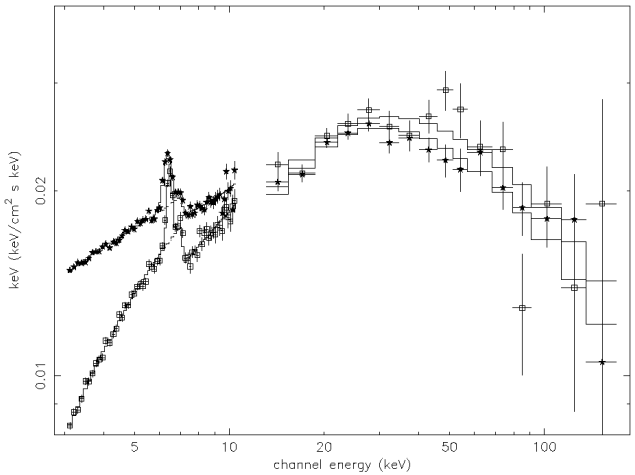

(Average Sy 1 and Sy 2 spectra from *BeppoSAX*; Malizia et al., 2003, Fig. 4)

Spectra of Sy 1 and Sy 2 are very similar, except for lower N_{H} in Sy 1

Variability

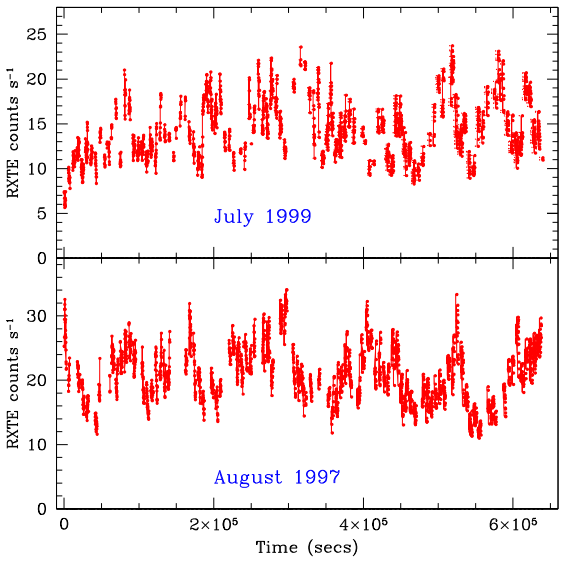

AGN are strongly variable

Timescale at $r_{\mathrm{ISCO}} = 6GM/c^2$:

$$t \sim \frac{2\pi r_{\mathrm{ISCO}}}{\sqrt{GM/r_{\mathrm{ISCO}}}} \propto \frac{r^{3/2}}{M^{1/2}} \propto M \qquad (9.4)$$

so less variable for higher BH mass.

(MGC−6-30-15; McHardy et al., 2005)

Relativistic Lines and BH Paradigm

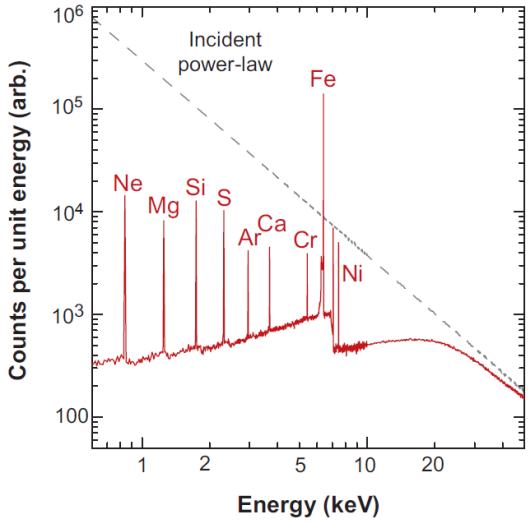

Prediction of neutral reflection models: fluorescent emission lines at low energies

(Reynolds, 1996)

Relativistic Lines and BH Paradigm

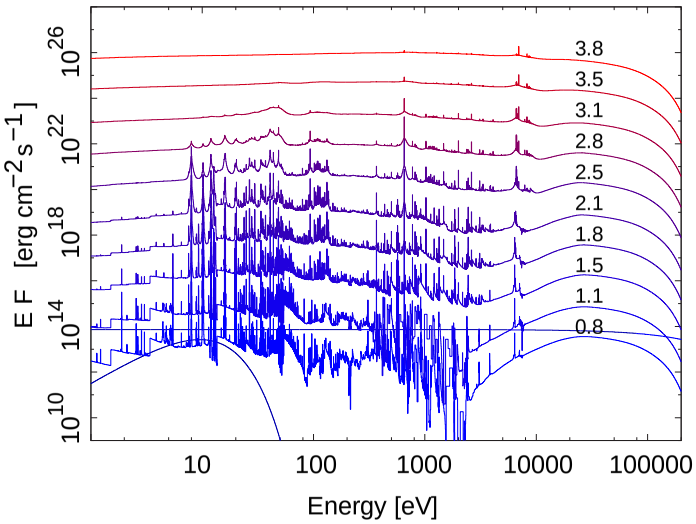

Ross & Fabian (2007, "`reflionx`"): Ionization: less absorption of lower Z elements $\Longrightarrow$ recovery of low energy emission, forest of emission lines

ionization parameter: $\xi = 4\pi F_x/n_{\mathrm{e}}$

Update with improved atomic physics: García & Kallman (2010), García et al. (2011)

(Fig. after García & Kallman, 2010)

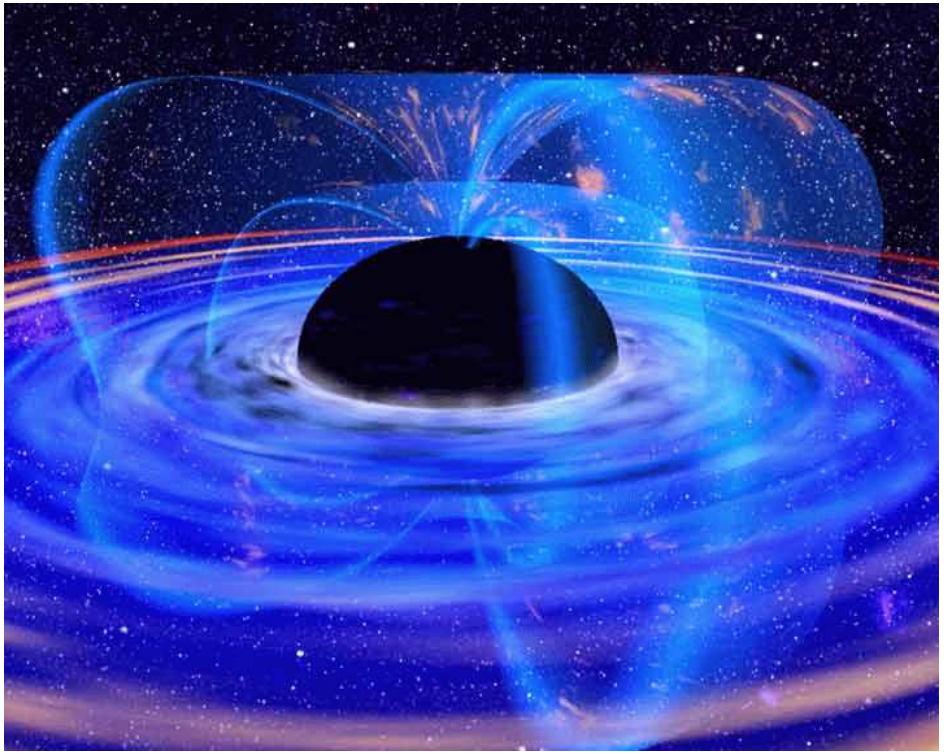

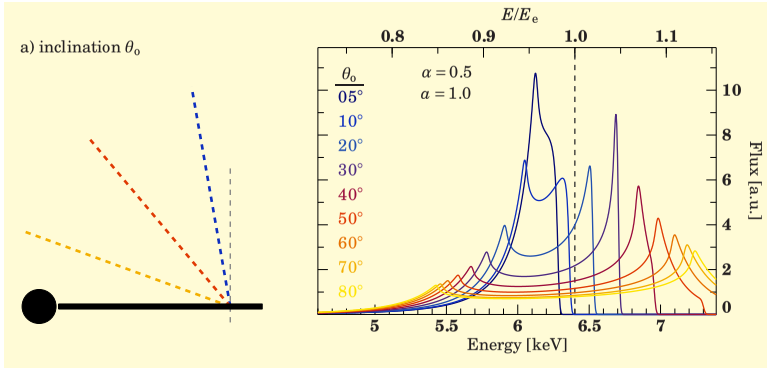

(Dauser, 2010)

Line profile has strong diagnostic potential: inclination

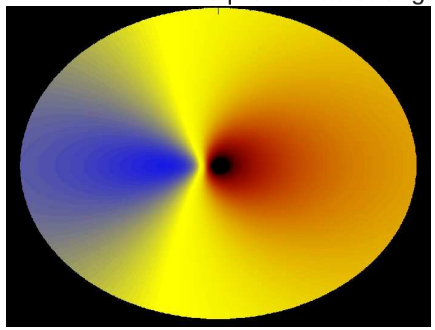

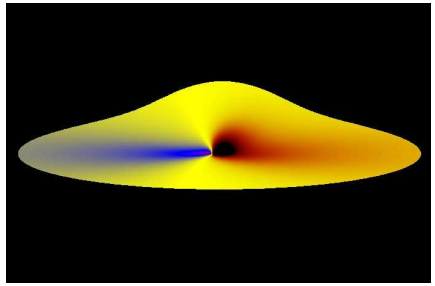

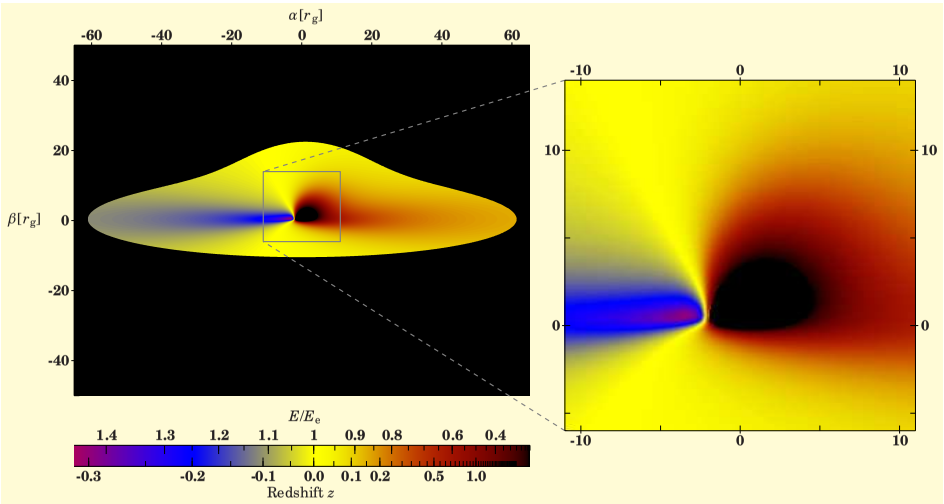

(Dauser, 2010)

Close to the black hole, we need to include relativistic effects: special relativistic beaming, light bending, and gravitational redshifts.

(Cunningham, 1975; Fabian et al., 1989; Laor, 1991; Dovčiak et al., 2004; Dauser et al., 2010)

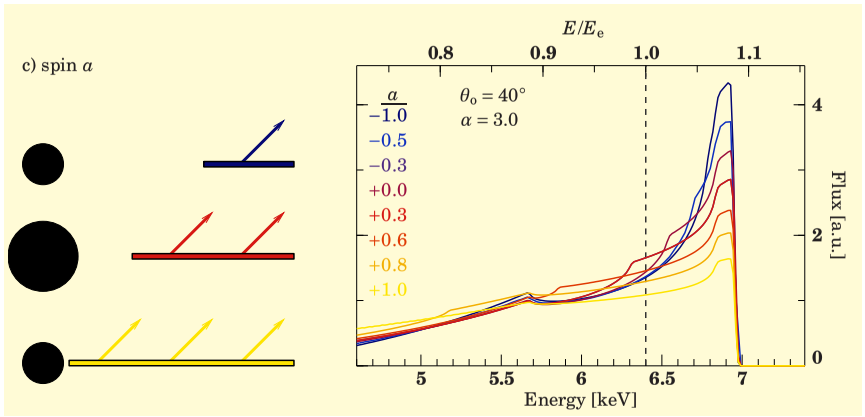

(Dauser, 2010)

Line profile has diagnostic potential: black hole spin (“holy grail”)

“negative spin”: angular momenta of disk and BH are antiparallel, also a stable configuration (King et al., 2008)

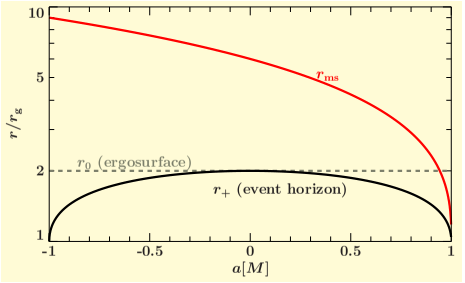

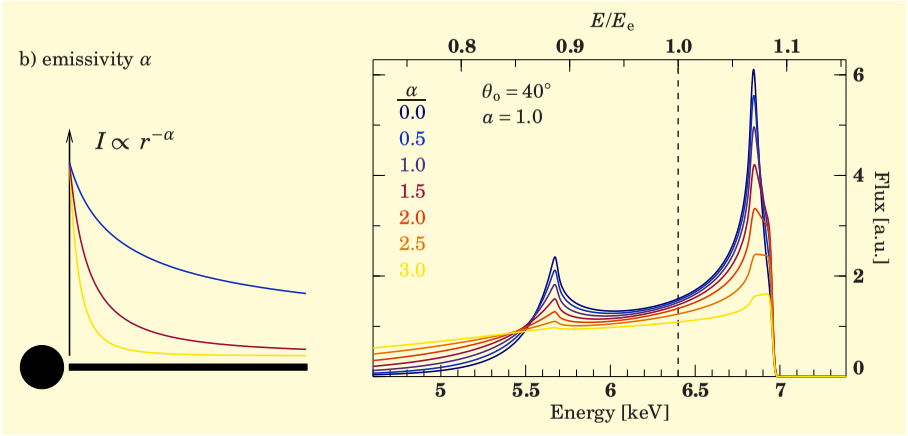

(Dauser, 2010)

Line profile has diagnostic potential: disk emissivity (=energy release per unit area)

for an α-disk: $\alpha \sim 3$

Relativistic Kα Lines

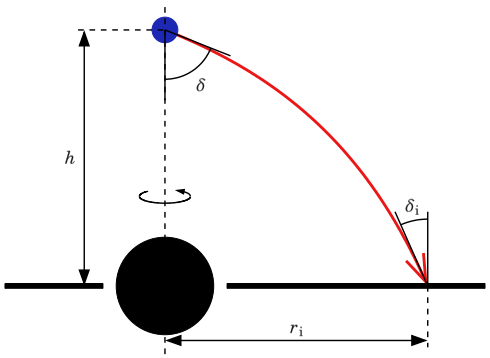

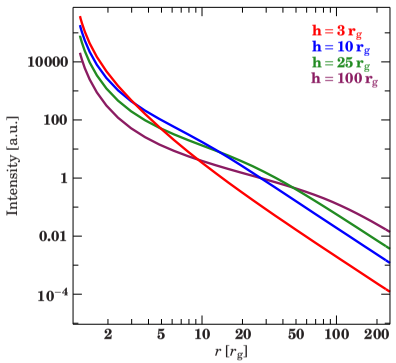

- Disks: emissivity α not well constrained
- Lamppost geometry: emissivity only depends on height above BH

Relativistic Smearing

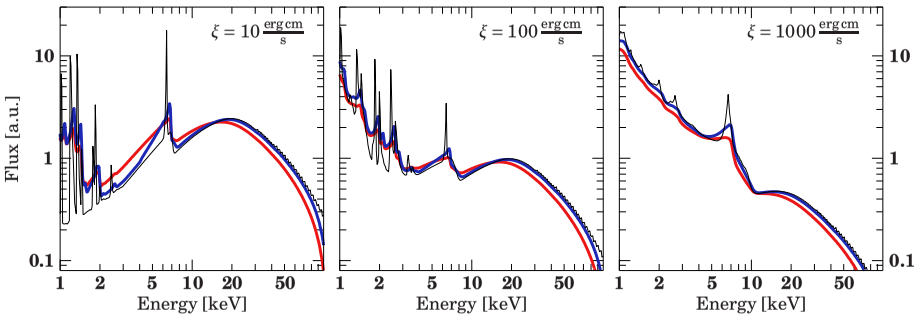

(Dauser, 2010)

Relativistic smearing affects the whole reflection spectrum

Only modeling a strong emission line with relativistic effects and ignoring the reflection continuum is wrong.

ASCA: MCG−6-30-15

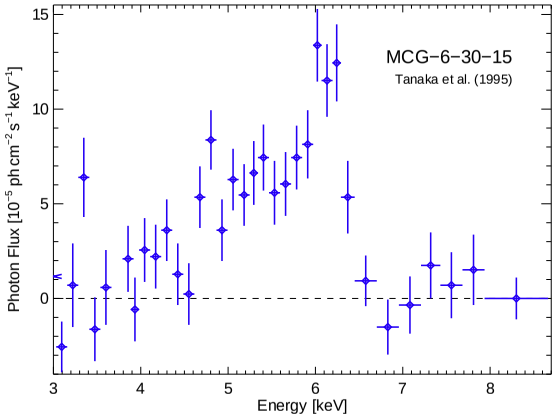

Tanaka et al. (1995): time averaged *ASCA* spectrum of Seyfert 1 MCG−6-30-15: line skew symmetric

$\Longrightarrow$ Schwarzschild black hole.

ASCA: MCG−6-30-15

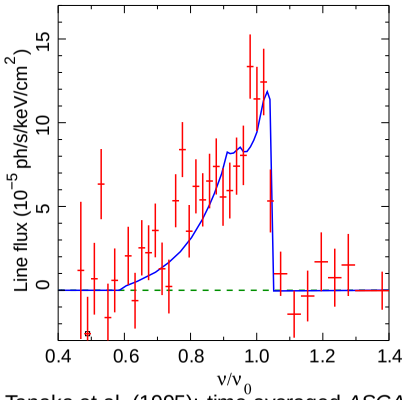

Tanaka et al. (1995): time averaged *ASCA* spectrum: line skew symmetric
$\Longrightarrow$ Schwarzschild black hole.

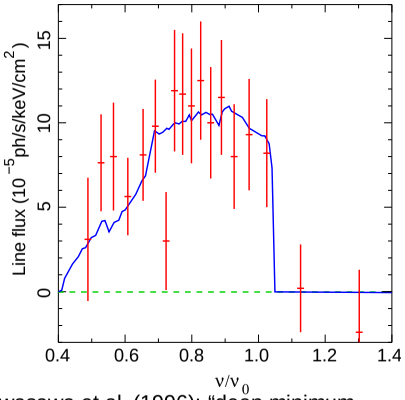

Iwasawa et al. (1996): "deep minimum state": extremely broad line
$\Longrightarrow$ Kerr Black Hole.

Later confirmed with *BeppoSAX* (Guainazzi et al., 1999) and *RXTE* (Lee et al., 1999).

XMM: MCG−6-30-15

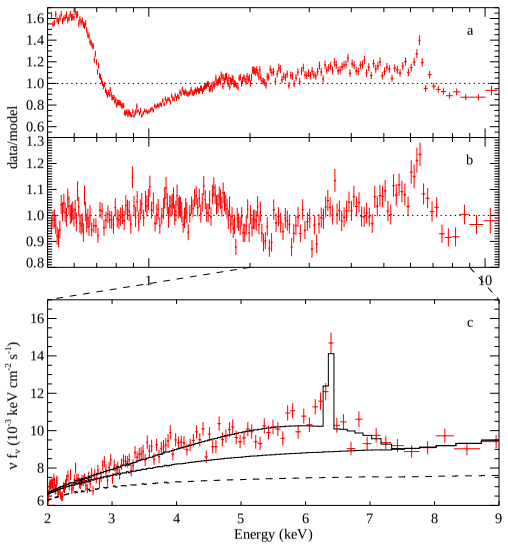

pure PL fit

Better modeling of soft excess and reflection $\Longrightarrow$ Fe Kα line has extreme width and skewed profile.

Components of the final fit.
$\Longrightarrow$ Line emissivity is strongly concentrated towards the inner edge of the disk ($\epsilon \propto r^{-4.6}$; cannot be explained with standard α-disk)

(*XMM-Newton*, June 2000, 100 ksec; Wilms et al., 2001)

XMM: MCG−6-30-15

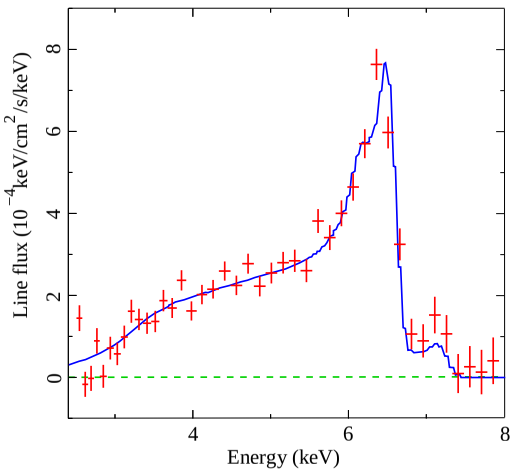

2001 July/August: 315 ksec observation
(Fabian et al., 2002)

- Strong narrow line
- broad line clearly present
- emissivity profile very steep for radii close to $r_{\rm in}$

$I_{\rm Fe\,K\alpha} \propto r^{-5.5\pm0.3}$ for $r < 6.1^{+0.8}_{-0.5} r_{\rm g}$,
$\propto r^{-2.7\pm0.1}$ outside that;
Fabian & Vaughan (2003); confirms Wilms et al. (2001)

Fabian et al. (2002)

XMM: MCG−6-30-15

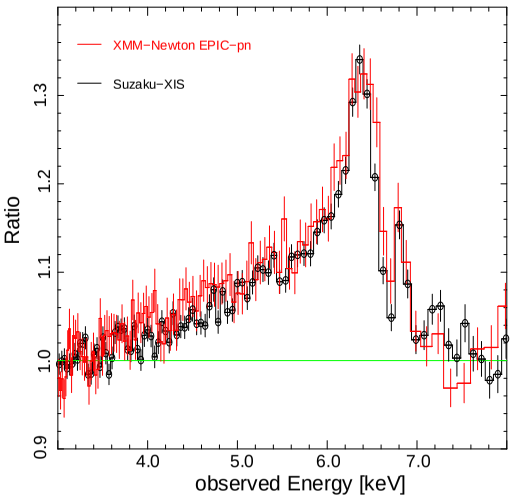

Brenneman & Reynolds (2006): Angular momentum of BH in MGC−6-30-15: $a = 0.989^{+0.009}_{-0.002}$.

Assuming no emission from inside the innermost stable circular orbit, strongly constrained geometry.

Suzaku (2006 Jan; ∼350 ksec; Miniutti et al., 2007)

Other Sources

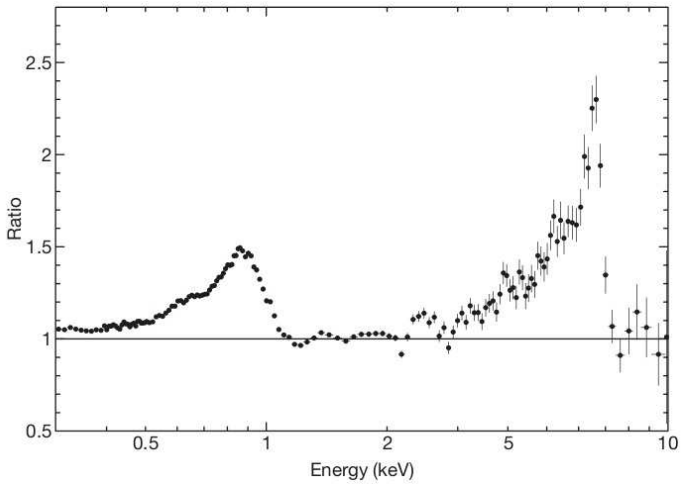

(Fabian et al., 2009)

1H0707−495 (NL Sy1): relativistically broadened Fe Kα *and* Lα lines; $a > 0.98$

Other Sources

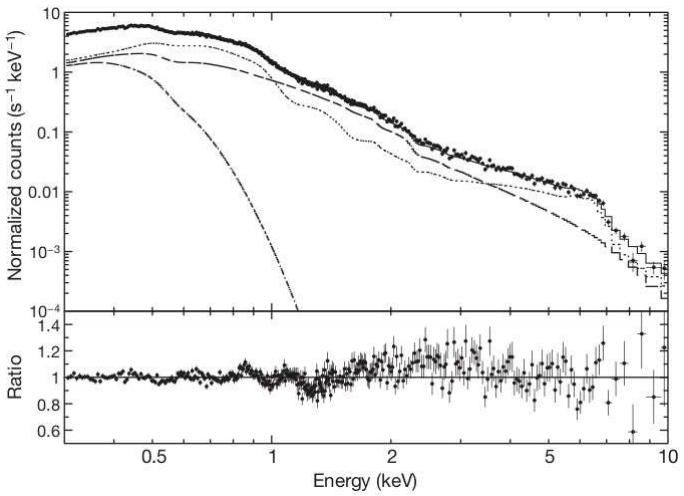

(Fabian et al., 2009)

1H0707−495 (NL Sy1): relativistically broadened Fe Kα *and* Lα lines; $a > 0.98$

Similar results also for IRAS13224−3809 (Ponti et al., 2010)

Other Sources

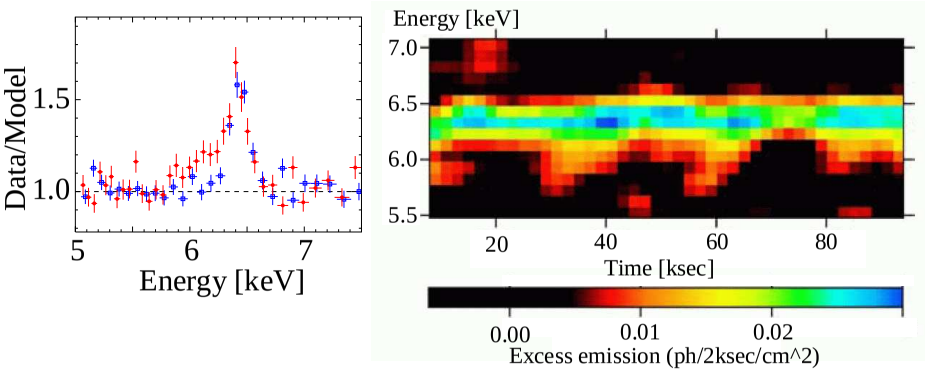

(Iwasawa et al., 2004, Figs. 3,4)

Line profile variability in NGC 3516 $\Longrightarrow$ Corotating flare? ($7r_g \lesssim r \lesssim 16r_g$)

If interpretation is pushed further, gives $M \sim (1 \ldots 5) \times 10^7\, M_\odot$.

Other Sources

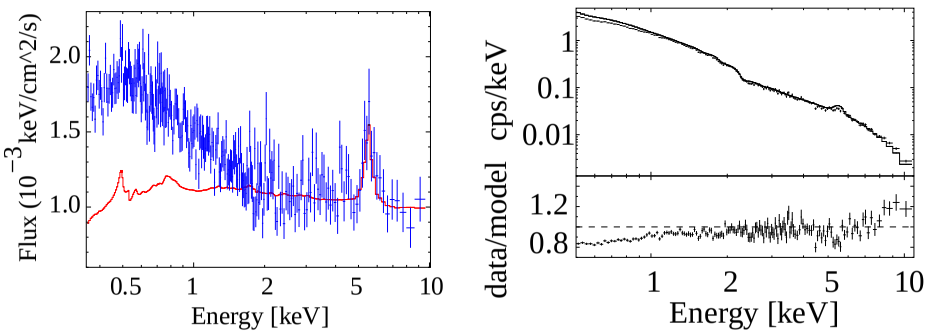

(Porquet & Reeves, 2003, Fig. 3)

XMM data from 2001

(Matt et al., 2005, Fig. 1)

comparison 2003 vs. 2001 data

Q0056−363 (broad line radio-quiet quasar, $L_X > 10^{45}$ erg s^{-1}):

Fe Kα has FWHM 24500 km s^{-1}, EW 275 eV

Q0056−363 is highest luminosity RQ-QSO with broad Fe Kα line.

Other Sources

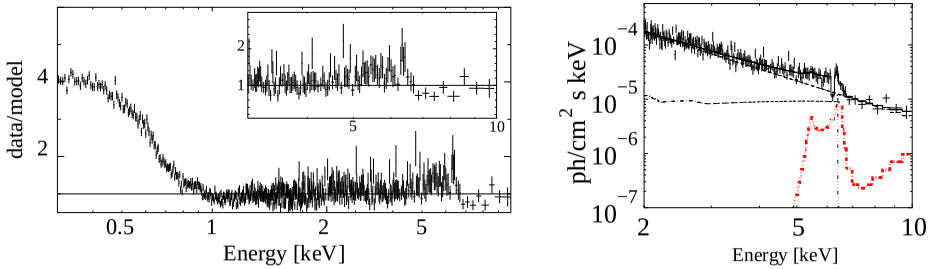

(Longinotti et al., 2003)

IRAS 13349+2436:

- Model either 2 broad emission lines *or*
- relativistic line from Fe XXIII/XXIV plus narrow absorption feature

Line shape can be rather complex!

Other examples include *blue*shifted lines, e.g., in Mkn 205 (Reeves et al., 2001) or Mkn 766.

Narrow Lines

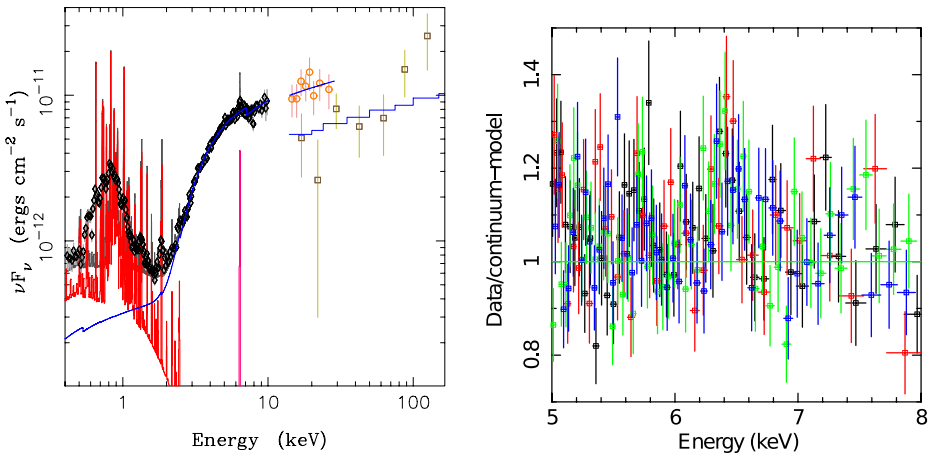

NGC 4258 (Reynolds, et al., 2008; Suzaku, Swift)

But: Some AGN do *not* show relativistic lines!

Narrow Lines

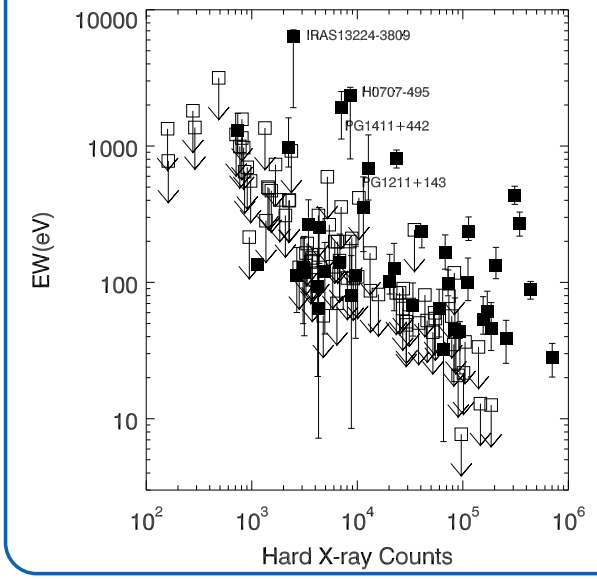

Guainazzi et al. (2006): non-detections due to ionization and detection significance

200000 photons are needed to unequivocally detect broad line in an AGN.

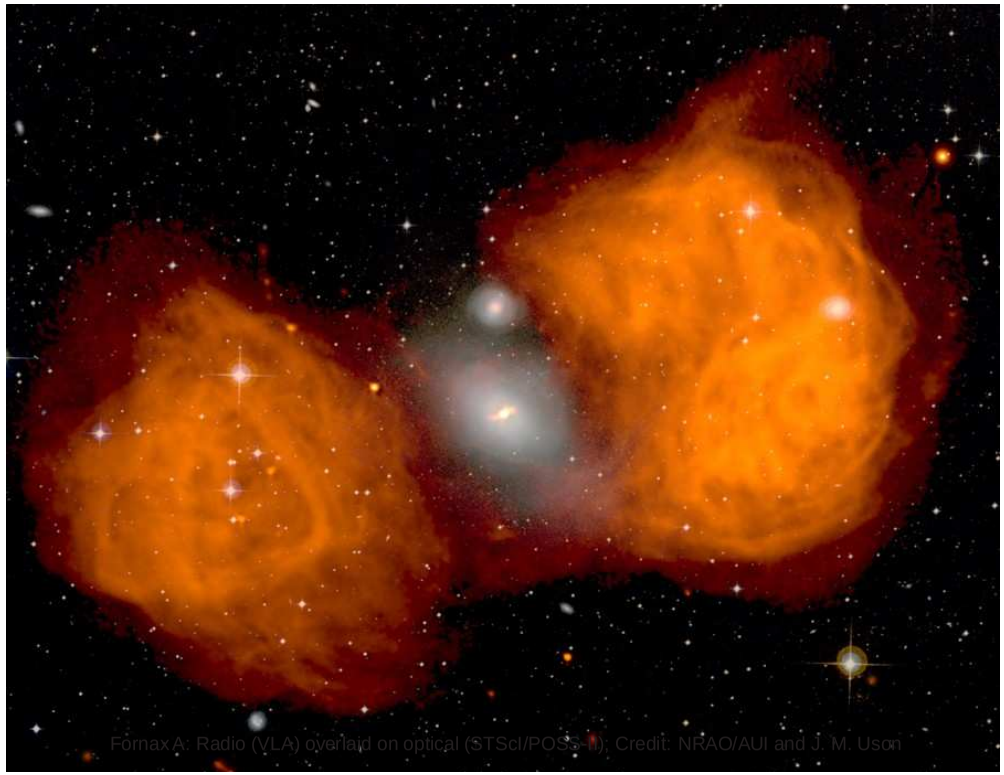

Classification

Radio-loud AGN are observed to have strong polarization and power law radio spectra. These are characteristics of synchrotron radiation.

Synchrotron-Radiation (=Magnetobremsstrahlung): Radiation emitted by relativistic electrons in a magnetic field.

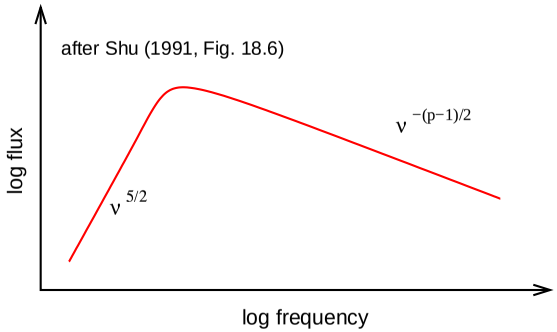

Spectrum of a single synchrotron-emitting blob:
At low ν: optically thick.
At high ν: optically thin.

Turnover: $\tau = 1$ surface

$\tau \propto R$ and $\nu(\tau = 1) \propto R^{-1}$

(R: size of the emitting region).

Classification

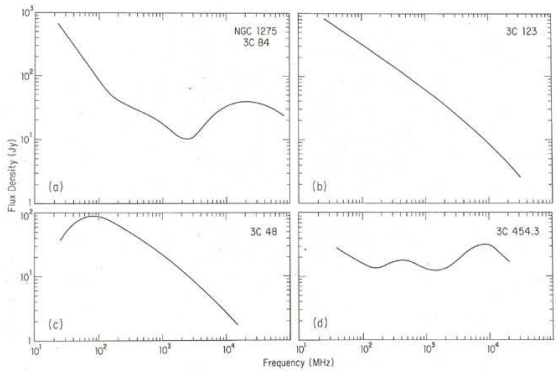

- NGC 1275: extended steep-spectrum emission plus compact self-absorbed nucleus
- 3C123: 3C 123: optically thin at all plotted frequencies
- 3C 48: self-absorbed below 100 MHz
- 3C454.3: superposition of many jet regions which become opaque at different frequencies (flat-spectrum radio quasar)

Classification

Classification of radio-loud AGN is based on morphology and radio spectrum:

1. Powerful double-lobed radio galaxies with hotspots and a steep radio spectrum falling toward higher frequencies (Fanaroff-Riley class II, FR II)
2. Weaker steep-spectrum, double-lobed radio galaxies without leading hotspots (FR I types)
3. Core-dominated flat-spectrum sources (Blazars: quasars and BL Lac objects)
4. Compact steep-spectrum sources (CSS sources) and gigahertz-peaked spectrum sources (GPS sources); no large-scale radio structure; morphological classification term: compact symmetric objects (CSOs) or compact doubles

Observing technique and frequency strongly affects sample (e.g., low-frequency flux-density limited surveys tend to select steep-spectrum sources). Flat-spectrum sources are classical targets for Very-Long-Baseline Interferometry (VLBI) observations, which are sensitive to compact emission.

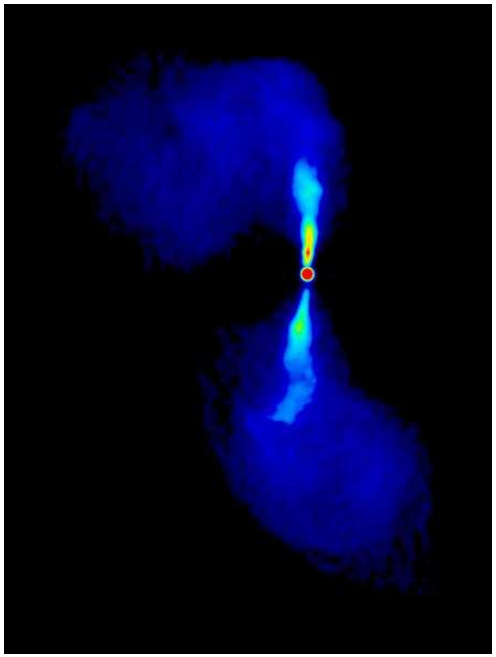

Fanaroff-Riley Type 1: asymmetric jets with wide opening angle ending in plumes

M84 (3C272.1) (Laing & Bridle, 1987):
VLA 4885 MHz, 134″ × 170″; see also
`www.jb.man.ac.uk/atlas/other/3C272P1.html`

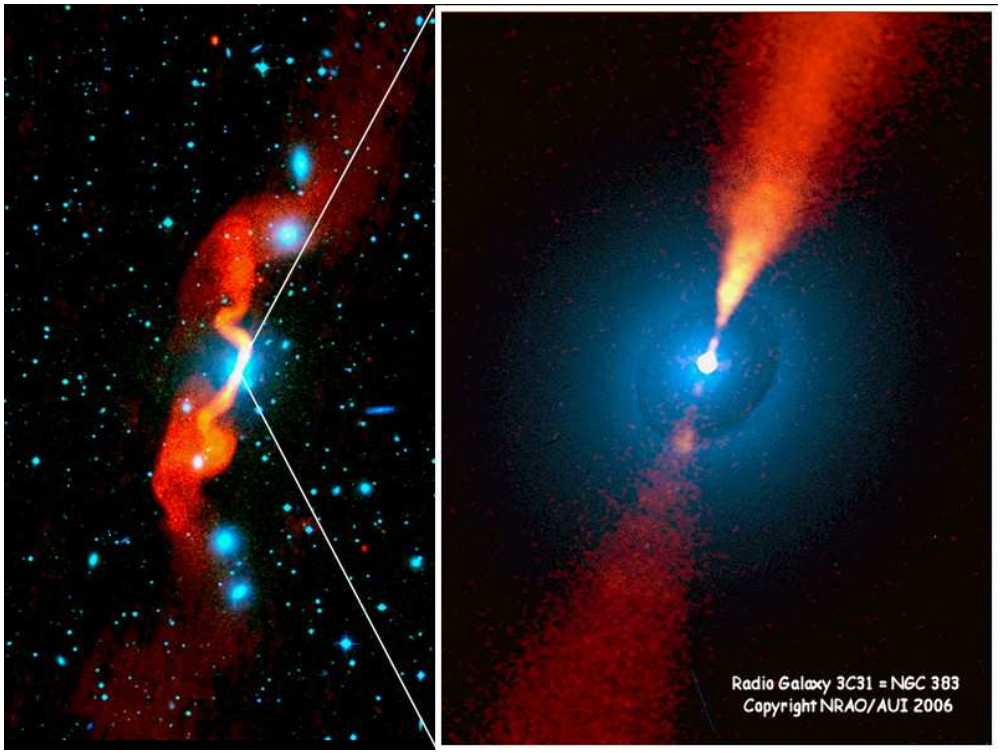

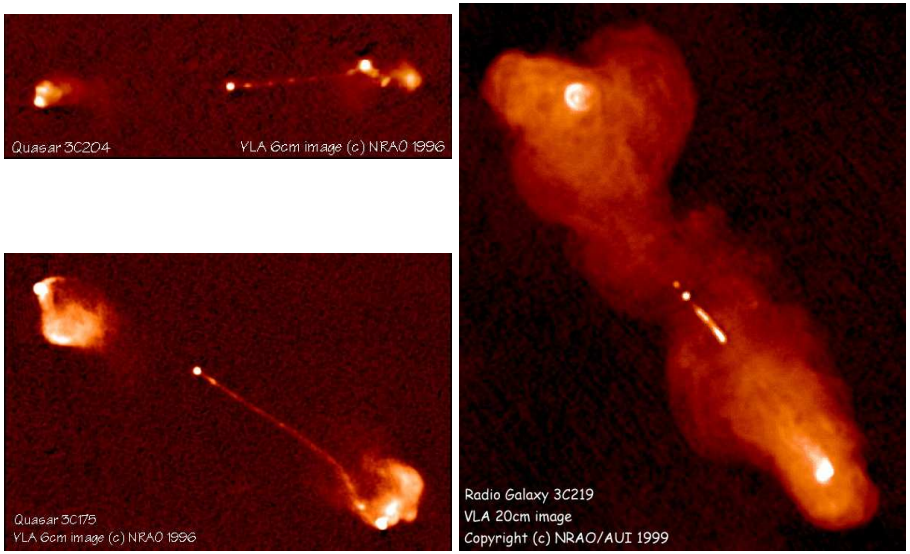

A. Bridle, `www.cv.nrao.edu/~abridle/images.htm`

Fanaroff-Riley Type 2: powerful lobe dominated doubles; jets often one-sided

Radio Interferometry: Longer baselines and higher frequencies yield higher resolution

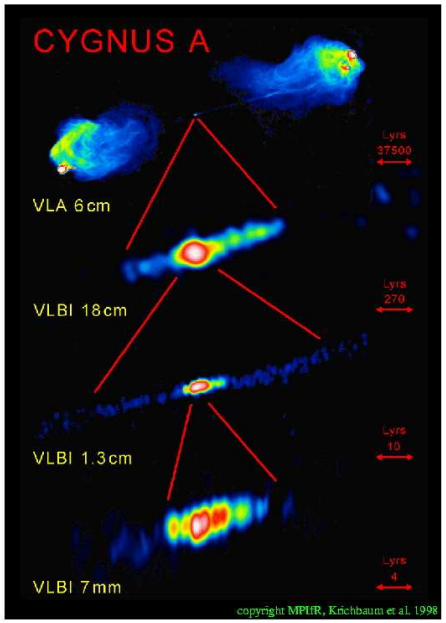

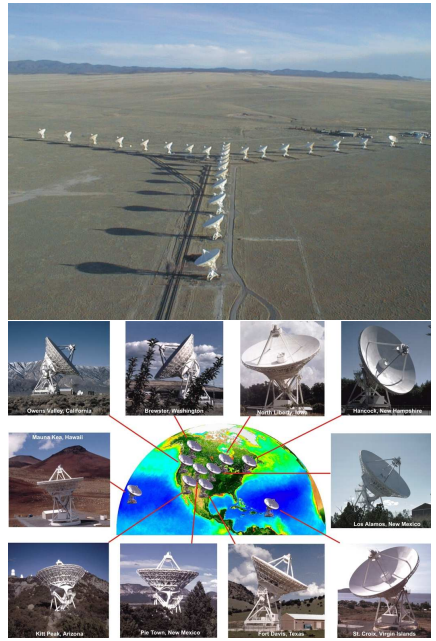

Image courtesy of MPIfR, NRAO/AUI and Earth image courtesy of the SeaWiFS Project NASA/GSFC and ORBIMAGE

Flat-Spectrum Radio Sources: Blazars

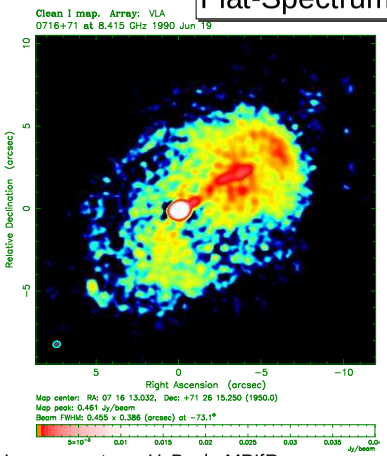

Image courtesy: U. Bach, MPIfR

0716+714: BL Lac at $z = 0.3$ (Nilsson et al., 2008)
Highly variable, core dominated object
"Fried-egg morphology": end-on view of a radio lobe?

Almost all flux density is concentrated within a few milliarcseconds-size compact jet!

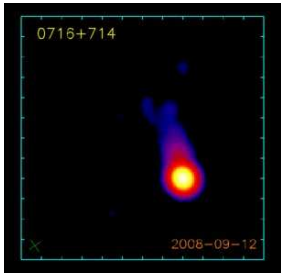

Image Courtesy: MOJAVE

"[There are] roughly equal numbers of steep-spectrum extended double-lobed sources and flat-spectrum objects that are unresolved on arc-sec scales." (Zensus, 1997)

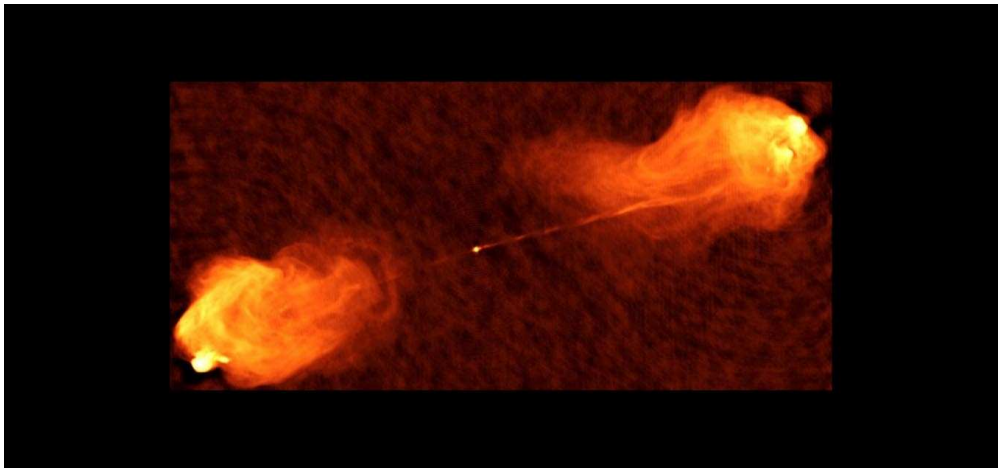

Cygnus A

Morphology of radio galaxies: matter is transported along two channels (jets) from the center of the system (core) to the outer regions (here: lobes): What is the speed?

Apparent Superluminal Motion

VLBI resolution 1 mas

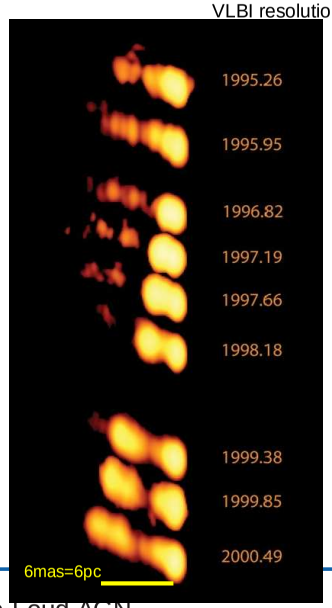

3C 111: Apparent speed of jet: $\sim 5c$

Superluminal motion: Apparent velocities of jet features ("blobs") in many AGN jets are $v > c$.

First discovered in 1971 in 3C279
(Cohen et al., 1971; Whitney et al., 1971).

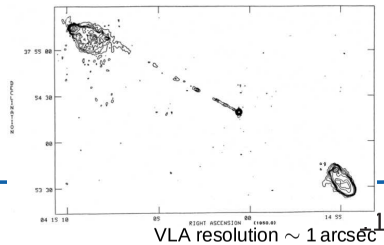

Kadler et al. (after 2008)

VLA resolution $\sim$ 1 arcsec

Apparent Superluminal Motion

Movies: Examples of superluminal motion in AGN jets

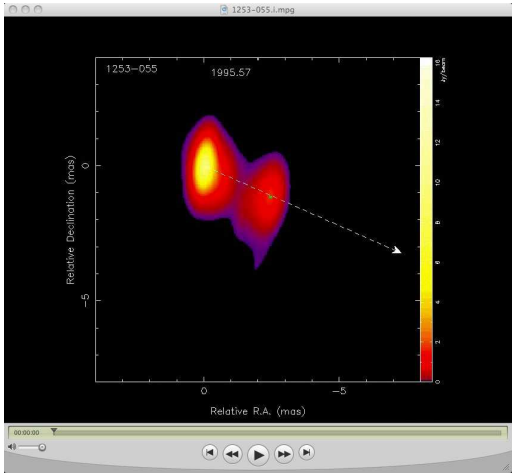

`http://www.physics.purdue.edu/astro/MOJAVE/movies.html`

Superluminal Motion Demo:

`www.physics.purdue.edu/MOJAVE/superluminal.swf`

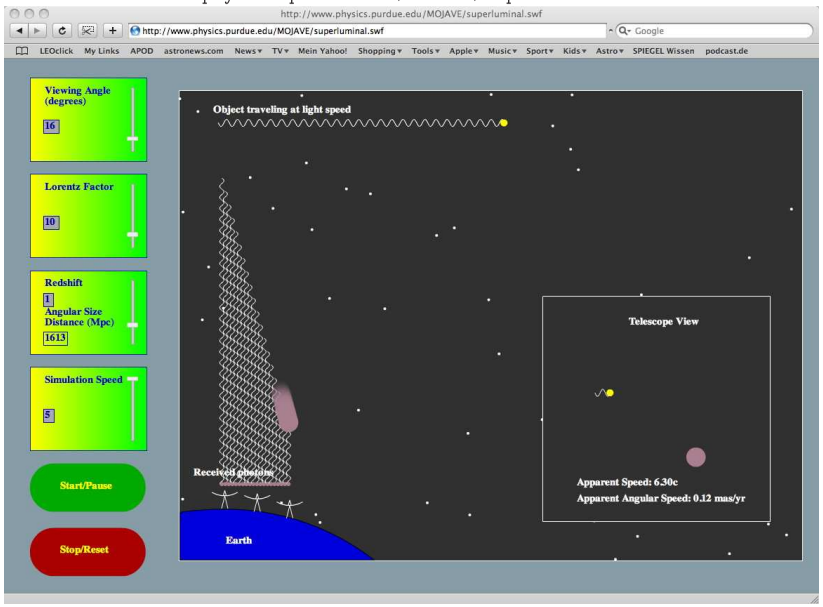

t_5: The last photons have a much shorter way to travel and arrive quickly. Observer measures superluminal motion on the sky!

Apparent Superluminal Motion

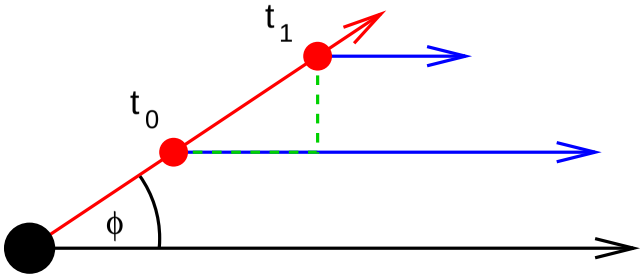

Consider blob moving towards us with speed v and angle ϕ with respect to line of sight, which emits signals at t_0 and $t_1 = t_0 + \Delta t_e$

Light travel time: Observer sees signals separated by

$$\Delta t_o = \Delta t_e - \Delta t_e \frac{v}{c} \cos\phi = \left(1 - \frac{v}{c}\cos\phi\right) \Delta t_e \qquad (9.5)$$

Observed distance traveled in plane of sky:

$$\Delta \ell_\perp = v \Delta t_e \sin\phi \qquad (9.6)$$

Apparent Superluminal Motion

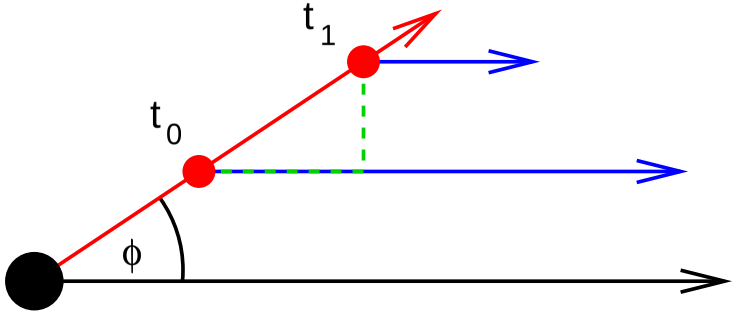

Apparent velocity deduced from observations:

$$v_{app} = \frac{\Delta \ell_\perp}{\Delta t_o} = \frac{v \Delta t_e \sin\phi}{\left(1 - \frac{v}{c}\cos\phi\right) \Delta t_e} = \frac{v \sin\phi}{\left(1 - \frac{v}{c}\cos\phi\right)} \qquad (9.7)$$

$\Longrightarrow$ For v/c large and ϕ small: $v_{app} > c$

Apparent Superluminal Motion

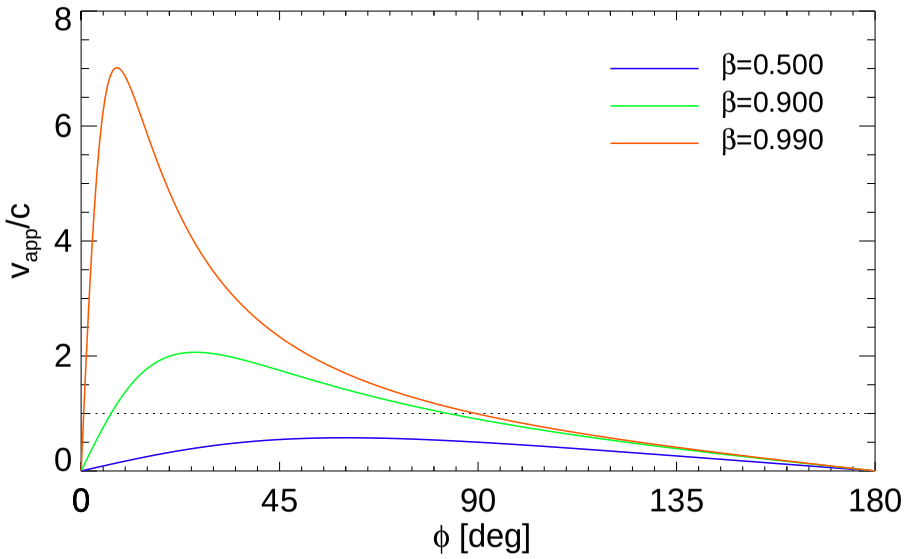

Relativistic Boosting

If jet plasma is moving at relativistic speeds, we have to consider also other relativistic effects.

Remember that (Doppler!)

$$\nu = \frac{1}{\Delta t_A} = \frac{\nu'}{\gamma\left(1 - \frac{v}{c}\cos\theta\right)} \quad \text{where} \quad \gamma = \frac{1}{\sqrt{1 - \frac{v^2}{c^2}}} \qquad (9.8)$$

This defines the relativistic Doppler factor

$$\mathcal{D} = \frac{1}{\gamma\left(1 - \frac{v}{c}\cos\theta\right)} = \frac{\sqrt{1-\beta^2}}{1 - \beta\cos\theta} \qquad (9.9)$$

(difference to classical Doppler factor is only the γ factor).

The Doppler factor is a strong function of the aspect angle and can become very large for $v \to c$.

Relativistic Boosting

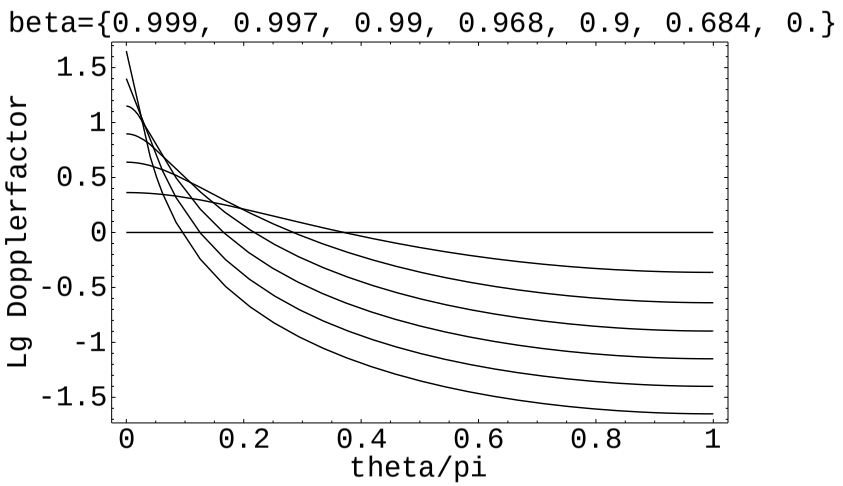

For $\theta \sim 1^\circ$–2°, the Doppler factor can approach values of 100 or higher.

Relativistic Boosting

One can show (i.e., Rybicki & Lightman, Ch. 4.9) that S_ν/ν^3 is invariant under Lorentz transformation, where S_ν is the flux density.

Therefore, observed intensity of a moving blob:

$$\frac{I(\nu_{\rm obs})}{\nu_{\rm obs}^3} = \frac{I(\nu_{\rm em})}{\nu_{\rm em}^3} \tag{9.10}$$

and

$$I(\nu_{\rm obs}) = \nu_{\rm obs}^3 \frac{I(\nu_{\rm em})}{\nu_{\rm em}^3} = \mathcal{D}^3 I(\nu_{\rm em}) \tag{9.11}$$

Specifically, for a blob with a power law spectrum ($I(\nu) = A\nu^\alpha$):

$$I(\nu_{\rm obs}) = \mathcal{D}^3 A \nu_{\rm em}^\alpha = \mathcal{D}^3 A \mathcal{D}^{-\alpha} \nu_{\rm obs}^\alpha \tag{9.12}$$

$$I(\nu_{\rm obs}) = \mathcal{D}^{3-\alpha} I(\nu_{\rm em}) \quad . \tag{9.13}$$

Even for relatively modest relativistic velocities, e.g., $0.97c$ ($\gamma \simeq 4$), forward flux can be boosted by a factor 1000, while it is reduced by a factor 1000 in the backward direction!

Jet One-Sidedness

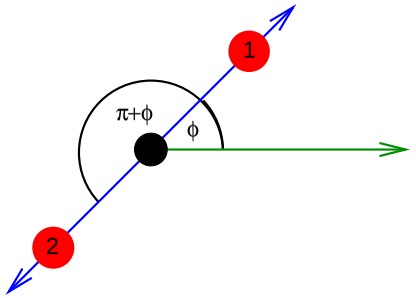

Take a source emitting blobs symmetrically in two directions.

From Eq. (9.12) the ratio of fluxes from the blobs is

$$\frac{F_1}{F_2} = \left(\frac{1+\beta\cos\phi}{1-\beta\cos\phi}\right)^{3-\alpha} \tag{9.14}$$

Even for mildly relativistic speeds and large angles, features on the approaching side are always significantly brighter than on the receding side.

Jet can be expressed as a series of blobs. But the number of blobs observed scales as the Doppler factor, such that for jets:

$$\frac{F_1}{F_2} = \left(\frac{1+\beta\cos\phi}{1-\beta\cos\phi}\right)^{2-\alpha} \tag{9.15}$$

One sidedness of jets is a relativistic effect!

Jet One-Sidedness

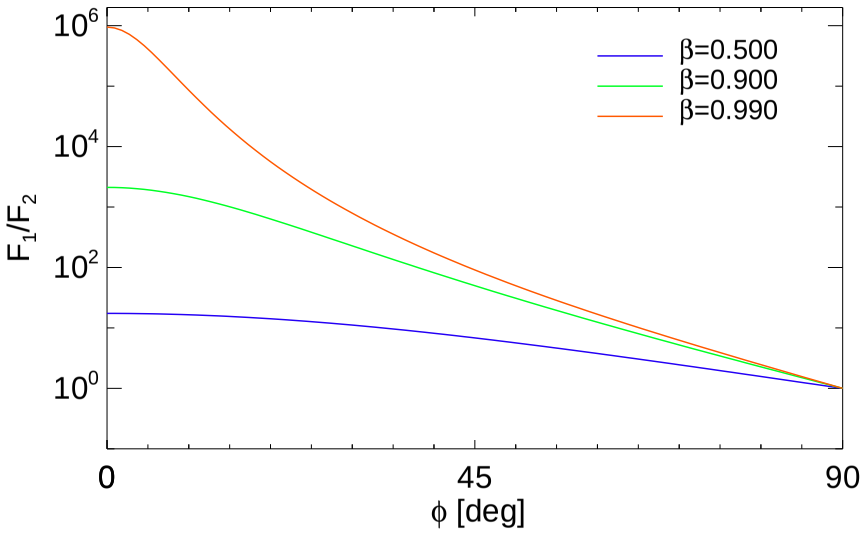

Survey and monitoring of extragalactic jets on parsec scales with the VLBA since 1995

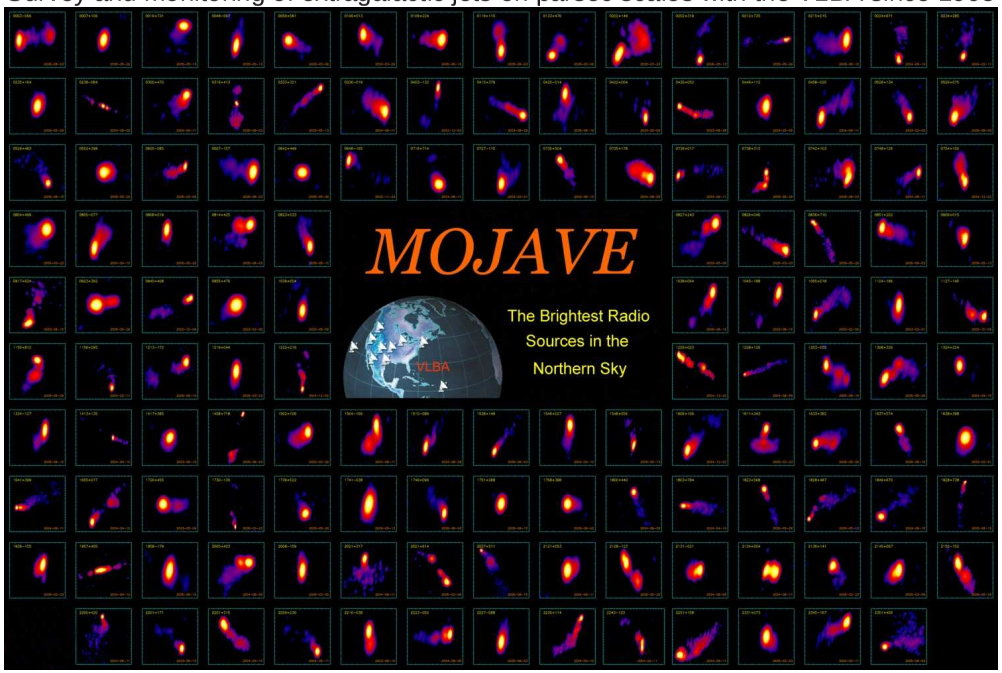

http://www.physics.purdue.edu/astro/MOJAVE/

Kinematics of Relativistic Jets

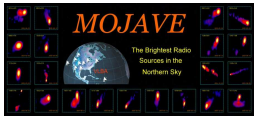

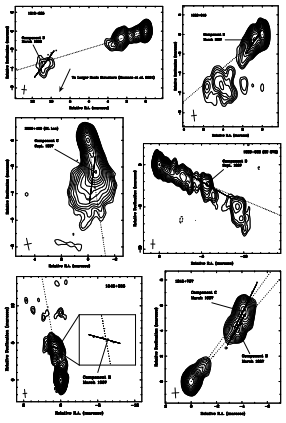

- **MOJAVE**: **M**onitoring **Of** **J**ets in **A**ctive galactic nuclei with **V**LBA **E**xperiments; (Lister et al., 2009, and therein)
- Wavelength $\lambda = 2\,\mathrm{cm}$ (15 GHz)
- Statistically complete sub-sample: All flat-spectrum ($\alpha < 0.5$) sources whose compact flux density ever reached 1.5 Jy (2 Jy for southern sources)
- Extended sample includes all known gamma-ray blazars (newly detected *Fermi* sources to be added as of January 2009)
- Results, images and movies at

  http://www.physics.purdue.edu/astro/MOJAVE/
- Observing strategy optimized for each individual source (fast sources are observed every month, slower sources less frequently)

Kinematics of Relativistic Jets

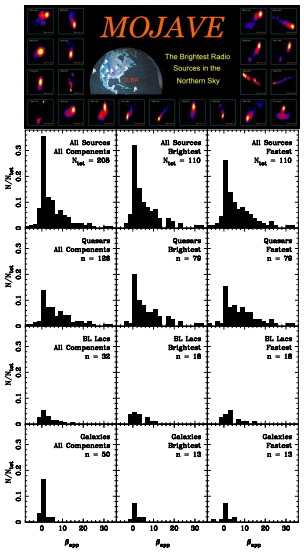

MOJAVE Results:

- Distribution of observed velocities typically between 0 and 15c: Quasars: tail up to $\beta_{\mathrm{app}} \sim 34$; BL Lacs and galaxies: mainly $\beta \lesssim 6$
- In the same jet, different components tend to have similar speeds; but there are exceptions
- In many sources, bent trajectories are seen, which do not back-extrapolate to the core: no cannon-balls!
- Observed pattern speed does not necessarily agree with beam speed
- Most of the flux-density originates in still unresolved regions smaller than 0.05 mas
- High-energy (gamma-ray) emitters have faster and more compact jets

(Kellermann et al., 2004; Kovalev et al., 2005; Cohen et al., 2007)

High Energy Radiation from Jets

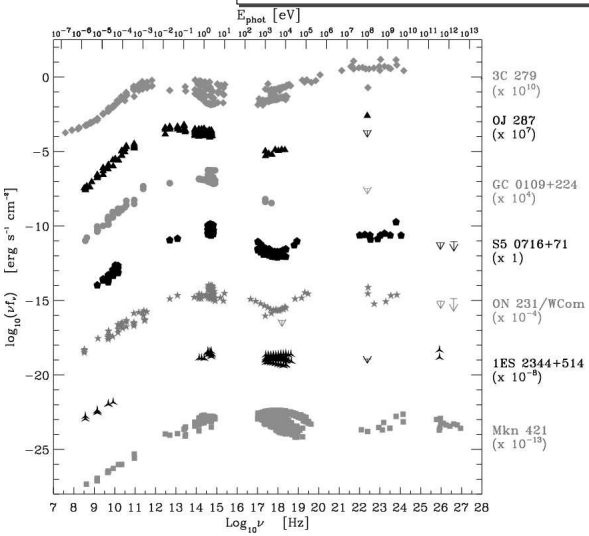

Sneak-preview of “blazar sequence” (Fiorucci et al., 2004)

Radio-loud AGN emit across the whole electromagnetic spectrum!

This holds for the compact and large-scale jets of both quasars and radio galaxies.

How can we transfer the power of the compact jet into high-energy emission?

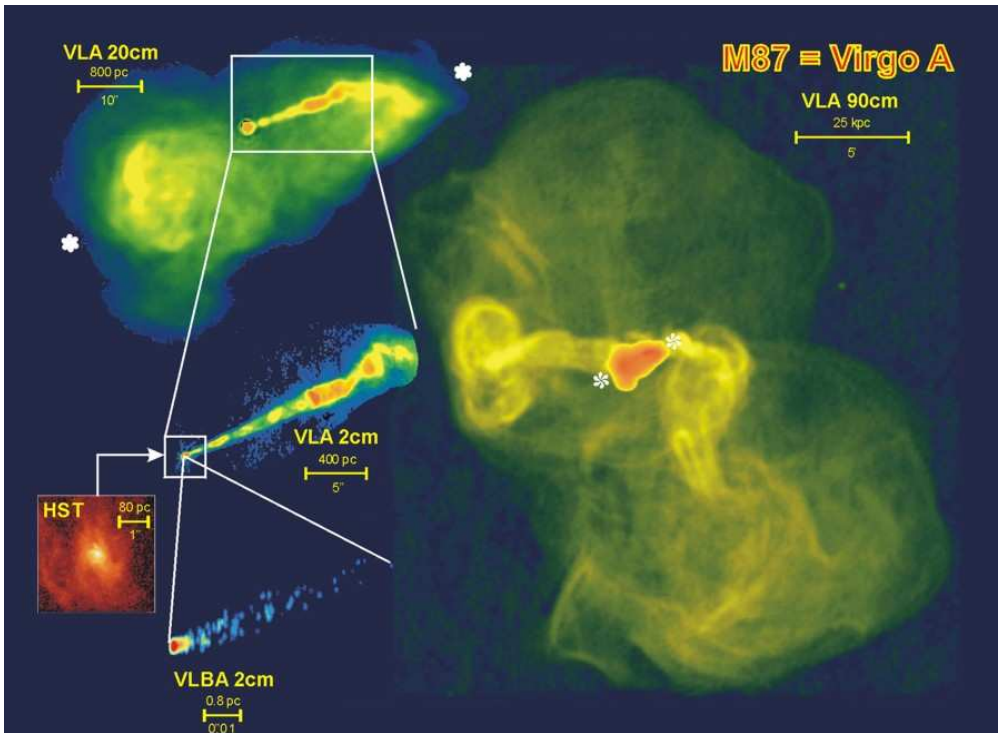
M87 = Virgo A
VLA 20cm
800 pc
10"
VLA 90cm
25 kpc
5'
VLA 2cm
400 pc
5"
HST
80 pc
1"
VLBA 2cm
0.8 pc
0.01


The M87 Jet
Hubble Heritage
PRC00-20 • Space Telescope Science Institute • NASA and The Hubble Heritage Team (STScI/AURA)

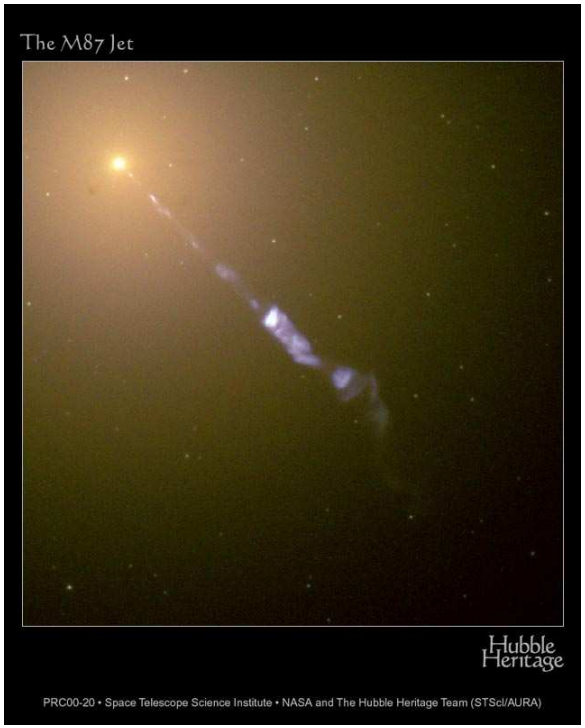
The M87 Jet
Hubble Heritage
PRC00-20 • Space Telescope Science Institute • NASA and The Hubble Heritage Team (STScI/AURA)

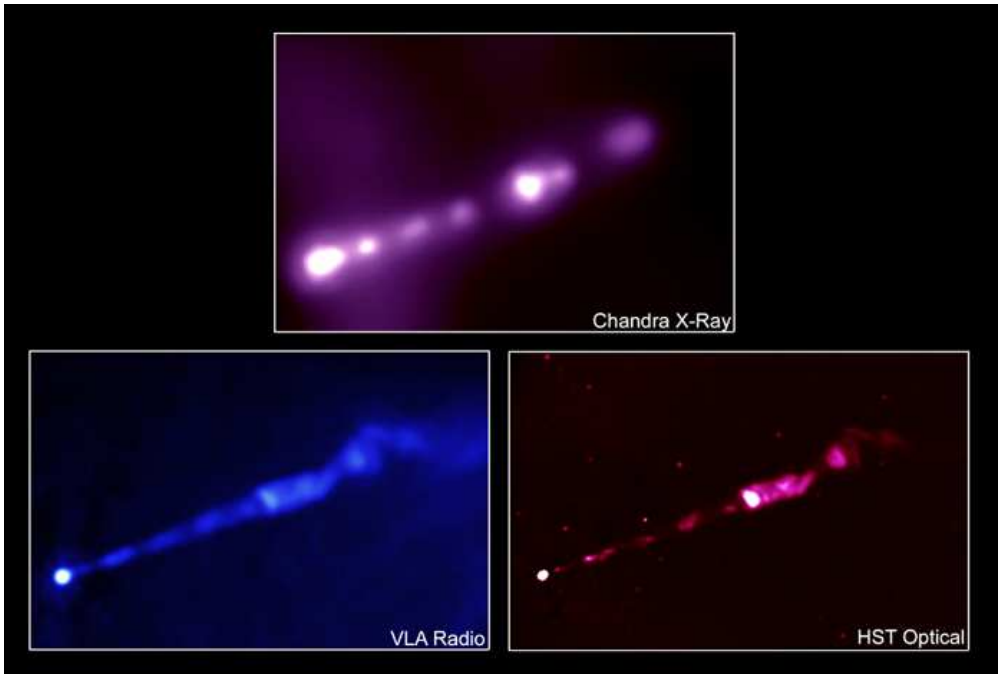
Chandra X-Ray
VLA Radio
HST Optical

High Energy Radiation from Jets

Blazars are broadband emitters and the most natural targets for multiwavelength astronomy!

The expression *Blazar* was first used in 1978 to express that optically violently variable quasars (OVVs) and BL Lac objects share their extreme variability characteristics.

Although first detected in optical and radio, a large fraction of their total energy output is at high energies: hard X-rays, γ-rays, and up to the very high energy (VHE) regime.

The *Compton Gamma-Ray Observatory (CGRO)* with its main detector EGRET revolutionized blazar research by the finding that blazars are the dominant population of extragalactic gamma-ray sources.

The short variability time scales (days!) indicate that the gamma-ray emission comes from beamed plasma (jets) to avoid photon-photon pair production in otherwise too dense gamma photon fields.

Prototypical Example: 3C 273

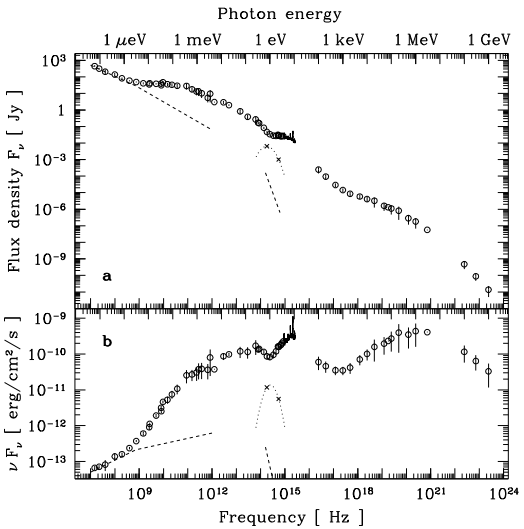

3C 273:

- First detected and brightest (and probably best studied) quasar
- Bright throughout the whole electromagnetic spectrum
- Prominent “big blue bump”
- Huge public database: Türler et al. (1999), Soldi et al. (2008)

(Türler et al., 1999)

Prototypical Example: 3C 273

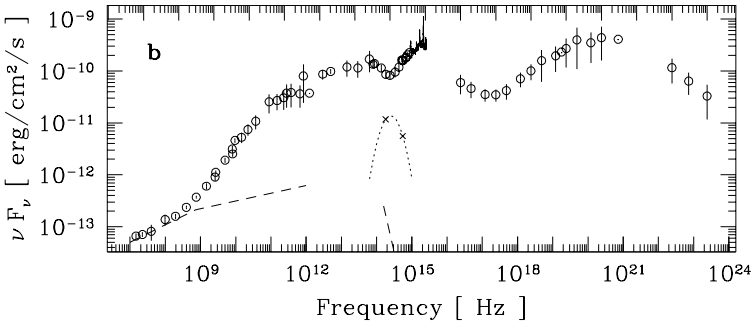

- Radio: low-frequency emission from large-scale jet; high-frequencies from compact jet (flat spectrum in F_ν)
- up to IR: synchrotron emission from compact jet (possibly plus dust component (dusty torus?))
- “big blue bump” in the optical: accretion disk (?)
- X-rays and up: inverse Compton emission (possibly from multiple seed photon fields)

Broadband Emission Models

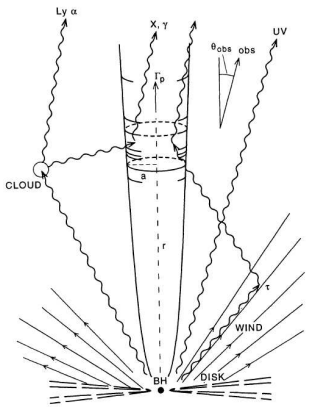

Geometry in leptonic models (Sikora et al., 1994)

General agreement that the low-energy component is jet-synchrotron emission.

Models for production of high energy photons:

- Leptonic models: inverse Compton scattering of soft seed photons by the relativistic electrons responsible for the synchrotron emission. Seed photons are
  - the synchrotron photons themselves (SSC, e.g. Tavecchio et al., 1998), or
  - external, e.g., from the accretion disk or the BLR (EC, e.g. Sikora et al., 1994)
- Hadronic models: reactions involving high-energy protons (hadron-hadron or photon-hadron collisions, pair production and subsequent e^+e^- cascades (e.g. Mannheim, 1993))

Hadronic models are attractive because they can explain the observed ultra-high energetic (UHE) cosmic rays but they have problems explaining the observed X-ray spectra.

Broadband Emission Models

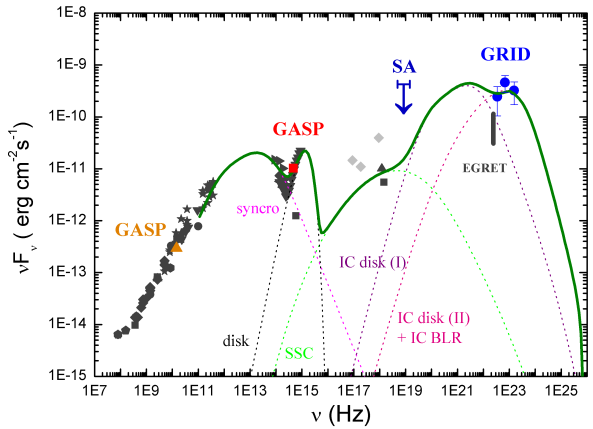

Modeling the broad-band SED:

- Consider primary components: synchrotron, disk, scattered BLR emission
- Inverse-Compton components from SSC and EC (of the dominating external photon fields)

SED of PKS B 1510−089 (Pucella et al., 2008)

Prototypical Example: 3C 273 (continued)

Almost 40 years of multiwavelength observations of 3C 273 (Soldi et al., 2008)

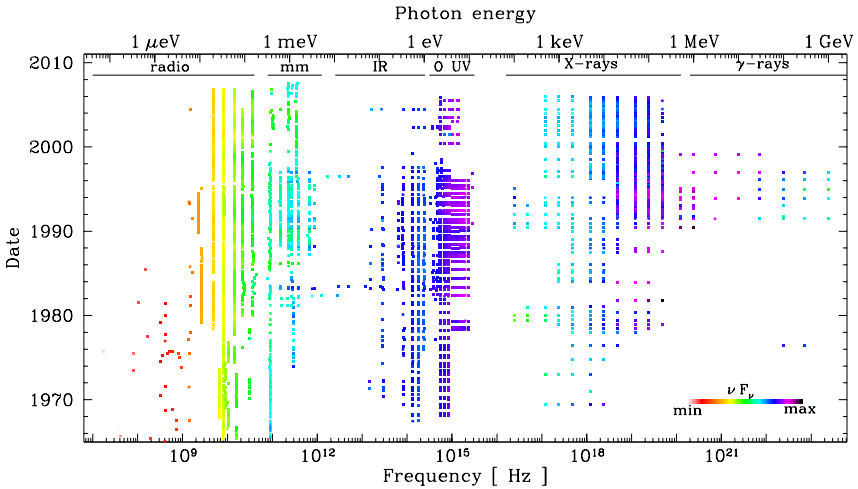

Prototypical Example: 3C 273 (continued)

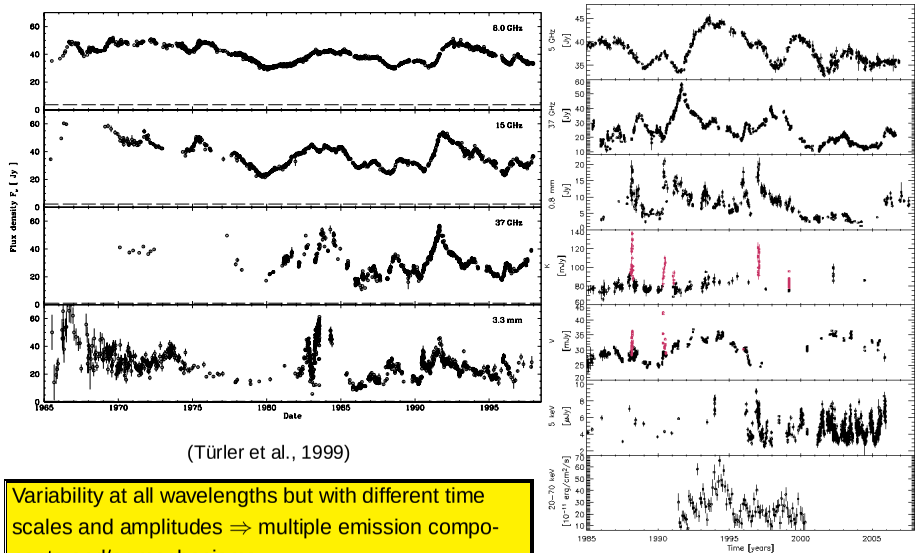

(Türler et al., 1999)

Variability at all wavelengths but with different time scales and amplitudes ⇒ multiple emission components and/or mechanisms

(Soldi et al., 2008)

Prototypical Example: 3C 273 (continued)

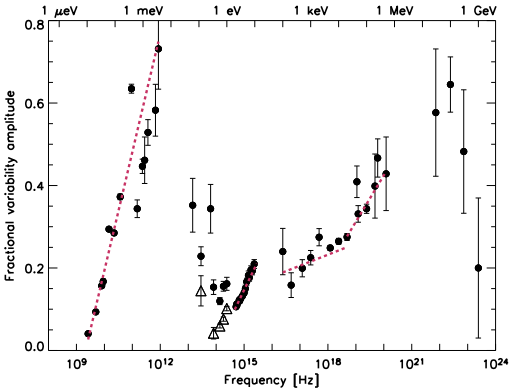

(Soldi et al., 2008)

Fractional variability amplitude:

$$F_{\rm var} = \sqrt{\frac{S^2 - \bar{\varepsilon}^2}{\bar{x}^2}} \qquad (9.16)$$

where: S^2: sample variance of the light curve, $\bar{x}$: average flux, and $\bar{\varepsilon}^2 = \frac{1}{N}\sum_i \varepsilon_i^2$: mean of the squared measurement uncertainties.

The fractional variability amplitude strongly depends on frequency, rising towards the high-energy end of the synchrotron and IC components. Less-variable IR emission (from dust?).

Prototypical Example: 3C 273 (continued)

Almost 40 years of multiwavelength observations of 3C 273 (Soldi et al., 2008)

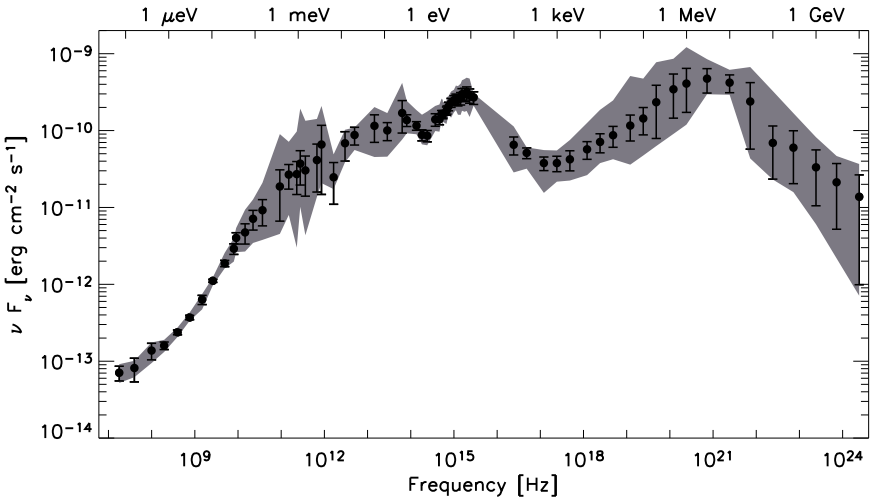

Prototypical Example: 3C 273 (continued)

A historic jet-emission minimum (Türler et al., 2006)

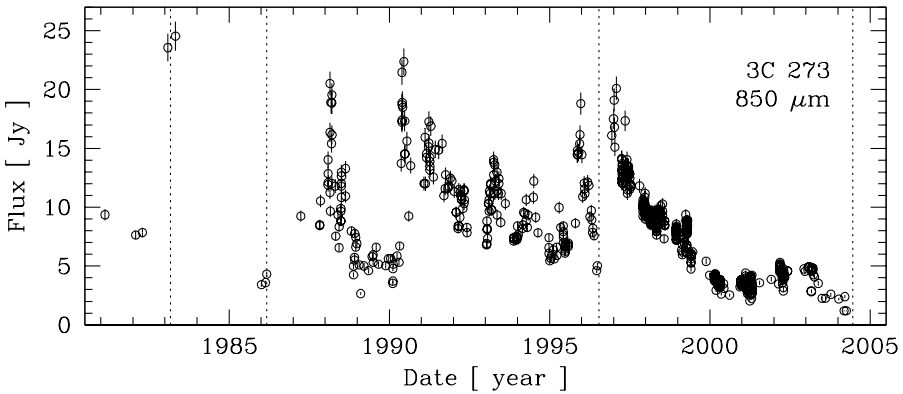

Prototypical Example: 3C 273 (continued)

A historic jet-emission minimum (Türler et al., 2006)

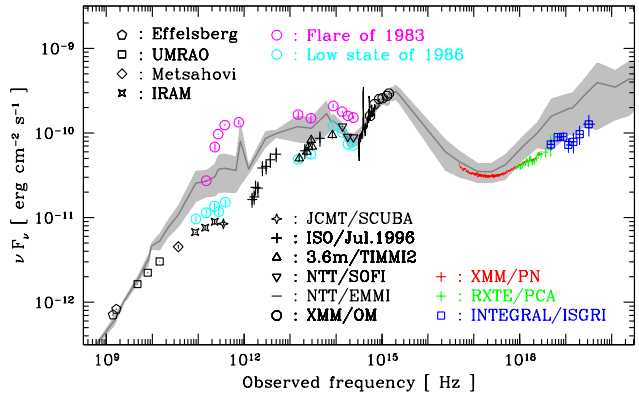

When the jet is weak, Seyfert-like features appear: Thermal dust, iron line; blue bump not directly coupled to jet emission

The Blazar Sequence

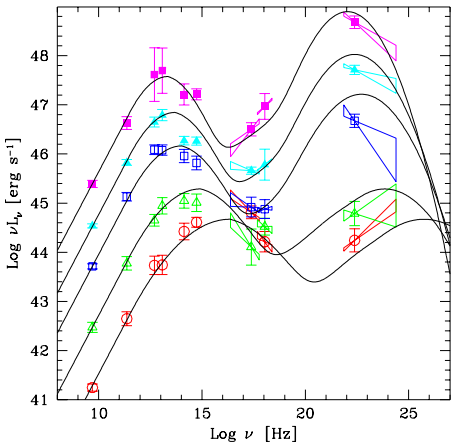

(Donato et al., 2001, based on Fossati et al. 1998)

Construction of average blazar SEDs binned according to radio luminosity (Fossati et al., 1998; Donato et al., 2001).
For all luminosity classes, there are two broad peaks

- LBL objects: High-luminosity sources peak at lower frequencies (IR and MeV range)
- HBL objects: Low-luminosity sources peak at higher frequencies (UV/X-rays and up to TeV energies)

The Blazar Sequence

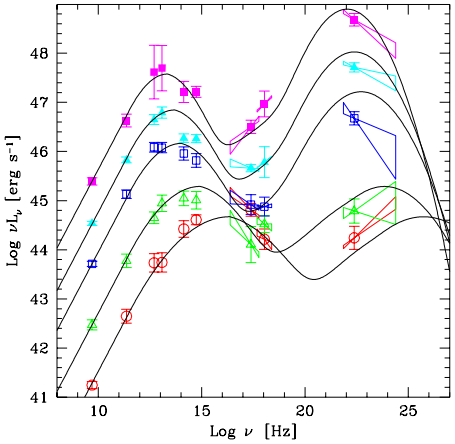

(Donato et al., 2001, based on Fossati et al. 1998)

Analytic parametrization:

- Peak frequencies are inversely proportional to luminosity
- Constant ratio of the two peak frequencies
- Strength of the second peak proportional to luminosity

Attention: EGRET detected preferentially blazars during outbursts ⇒ Bias in high-energy data.

There is an ongoing debate on the validity of the blazar sequence. A (small) number of sources does not fit in.

Blazars at γ-Ray Energies

Third EGRET Catalog
E > 100 MeV

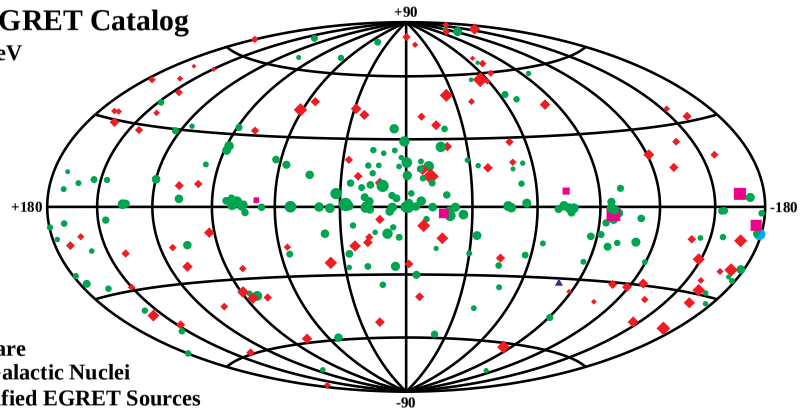

- ▲ LMC
- ■ Pulsars
- ● Solar Flare
- ◆ Active Galactic Nuclei
- ● Unidentified EGRET Sources

Hartman et al. (1999): 271 sources – 5 pulsars, 1 solar flare, 93 blazars (66 high confidence, 27 possible associations), 1 radio galaxy, 1 normal galaxy, and 170 (!) unidentified sources.

Blazars at γ-Ray Energies

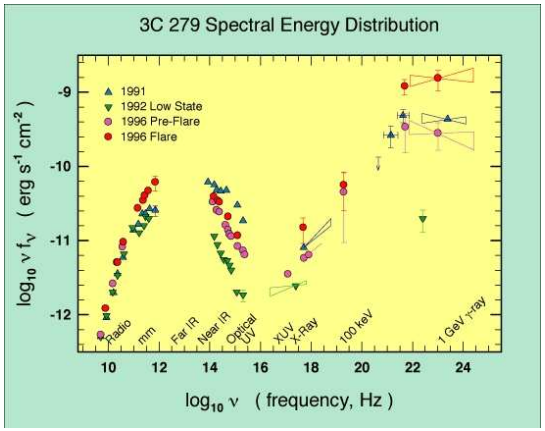

Courtesy: EGRET Team

Blazar SED dominated by γ-ray emission.

Example 3C 279:

- Surprise! (observation was looking for 3C 273)
- Became the prototypical γ-ray blazar through the whole EGRET mission

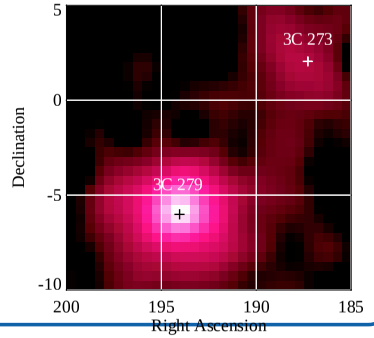

Blazars at γ-Ray Energies

The elusive gamma-ray regime is now much better covered than ever before:

Agile launched in April 2007. Now in routine pointed observations mode.

`http://agile.rm.iasf.cnr.it/`

GLAST (Gamma Ray Large Area Space Telescope) launched in June 2008. Now renamed to *Fermi Gamma-Ray Space Telescope* and in routine all-sky monitoring mode.

`http://fermi.gsfc.nasa.gov/`

Fermi Gamma-ray Space Telescope

Blazars at γ-Ray Energies

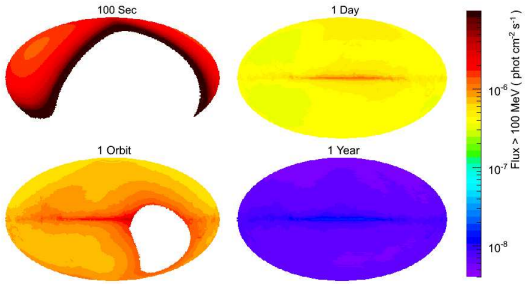

Primary observing mode of the LAT is *survey mode*:

- Full sky coverage every 2 orbits (3 hours)
- $\sim$ Uniform exposure after a couple of orbits
- Sensitivity of previous γ-ray missions reached within $\sim$1 week

Comparison with EGRET:

- Very large field of view ($\sim$ 20 % of the sky)
- Broadband (20 MeV – >300 GeV)
- PSF <1 degree (energy dependent)
- Effective area >8000 cm^2

Overall: Factor > 30 improvement in sensitivity!

Gamma-ray Space Telescope

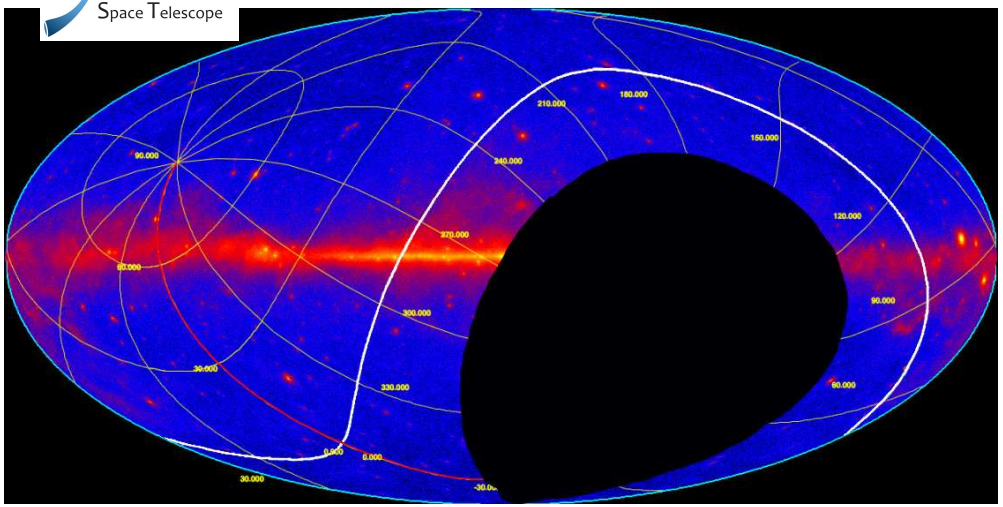

One third of the sky is not observable for Northern-Hemisphere Telescopes!

Gamma-ray Space Telescope

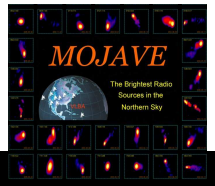

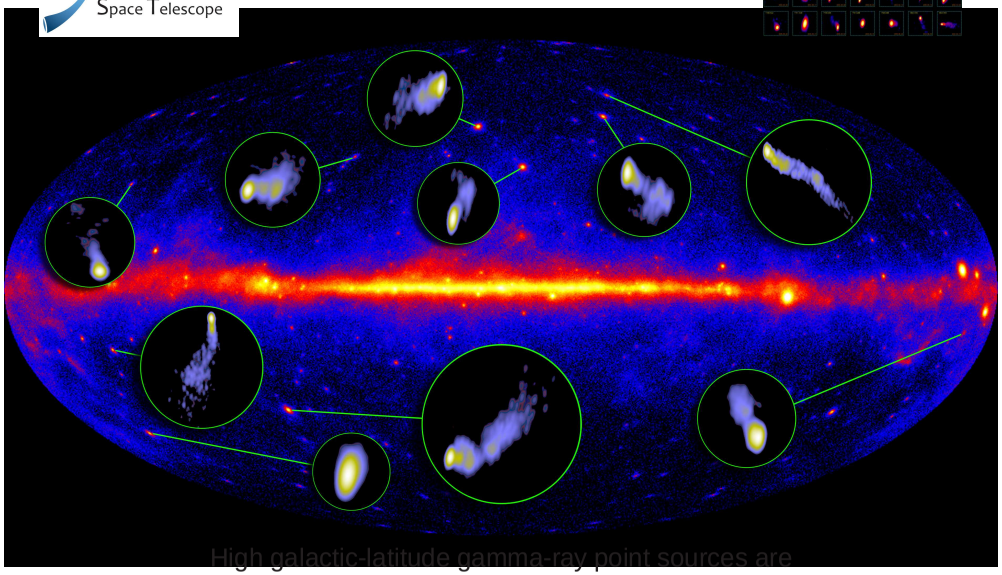

High galactic-latitude gamma-ray point sources are flat-spectrum radio quasars and BL Lac objects

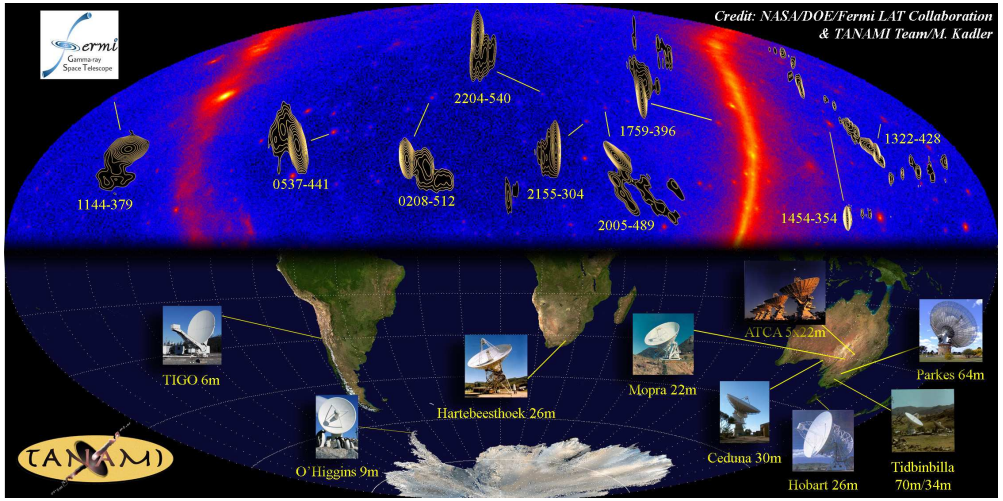

TANAMI (Tracking Active Galactic Nuclei with Austral Milliarcsecond Interferometry)
http://pulsar.sternwarte.uni-erlangen.de/tanami

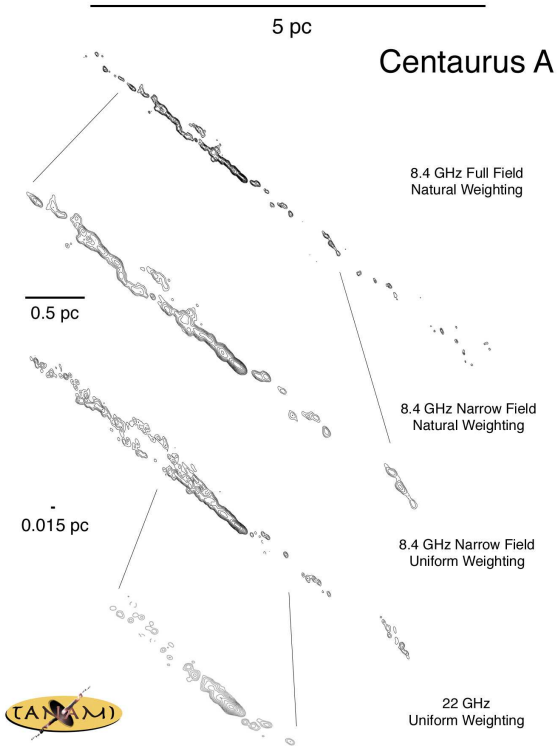

Blazars at Very High Energies

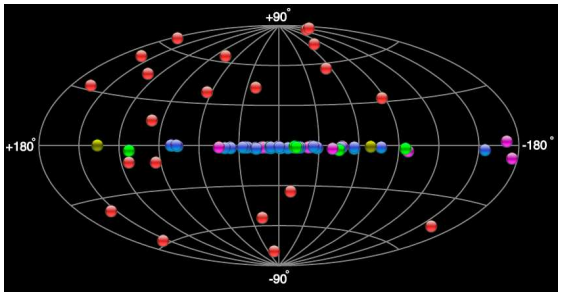

The blazar sequence predicts a dominance of HBL objects at very high energies. This is confirmed by recent blazar detections of TeV telescopes (H.E.S.S., MAGIC, VERITAS, CANGAROO):

- Currently 22 HBL objects detected and only two LBL objects (W Comae and BL Lac; check `http://tevcat.uchicago.edu/` for updated lists)
- Only non-blazar TeV source: M 87

Blazars at Very High Energies

TeV blazars are weak radio sources, because the cm-range is so far left of their synchrotron peak and because they are low-luminosity objects. Similarly, they are bright X-ray sources and relatively weak in the MeV/GeV range.

Despite their variability and SEDs require very high Doppler factors, VLBI measures slow jets (barely superluminal Piner et al., 2008, and references therein) ⇒ 1) extremely small angles or 2) jet deceleration from the “blazar scale” to the “VLBI scale”, or 3) another sign of jet-stratification (spine-sheath structure).

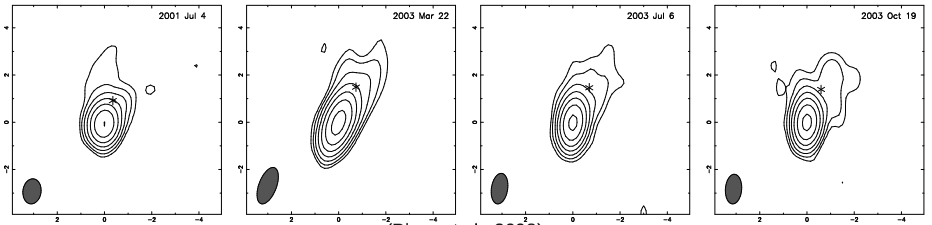

(Piner et al., 2008)

Baade W., Minkowski R., 1954, ApJ 119, 206
Cohen M.H., Cannon W., Purcell G.H., et al., 1971, ApJ 170, 207
Cohen M.H., Lister M.L., Homan D.C., et al., 2007, ApJ 658, 232
Cunningham C.T., 1975, ApJ 202, 788
Dauser T., 2010, Diplomarbeit, Universität Erlangen-Nürnberg
Dauser T., Wilms J., Reynolds C.S., Brenneman L.W., 2010, MNRAS 409, 1534
Donato D., Ghisellini G., Tagliaferri G., Fossati G., 2001, A&A 375, 739
Dovčiak M., Karas V., Yaqoob T., 2004, ApJS 153, 205
Fabian A.C., Rees M.J., Stella L., White N., 1989, MNRAS 238, 729
Fabian A.C., Ross R.R., 2010, Space Sci. Rev. 157, 167
Fabian A.C., Vaughan S., Nandra K., et al., 2002, MNRAS 335, L1
Fabian A.C., Zoghbi A., Ross R.R., et al., 2009, Nat 459, 540
Fiorucci M., Ciprini S., Tosti G., 2004, A&A 419, 25
Fossati G., Maraschi L., Celotti A., et al., 1998, MNRAS 299, 433
García J., Kallman T.R., 2010, ApJ 718, 695
García J., Kallman T.R., Mushotzky R.F., 2011, ApJ 731, 131
García-Lorenzo B., Mediavilla E., Arribas S., 1999, ApJ 518, 190
Guainazzi M., Bianchi S., Dovčiak M., 2006, Astron. Nachr. 327, 1032
Guainazzi M., Matt G., Molendi S., et al., 1999, A&A 341, L27
Guilbert P.W., Rees M.J., 1988, MNRAS 233, 475
Hartman R.C., Bertsch D.L., Bloom S.D., et al., 1999, ApJS 123, 79
Iwasawa K., Fabian A.C., Reynolds C.S., et al., 1996, MNRAS 282, 1038
Iwasawa K., Miniutti G., Fabian A.C., 2004, MNRAS 355, 1073
Kadler M., Ros E., Perucho M., et al., 2008, ApJ 680, 867
Kellermann K.I., Lister M.L., Homan D.C., et al., 2004, ApJ 609, 539
King A.R., Pringle J.E., Hofmann J.A., 2008, MNRAS 385, 1621
Kovalev Y.Y., Kellermann K.I., Lister M.L., et al., 2005, AJ 130, 2473
Laing R.A., Bridle A.H., 1987, MNRAS 228, 557
Laor A., 1991, ApJ 376, 90
Lee J.C., Fabian A.C., Brandt W.N., et al., 1999, MNRAS 310, 973
Lightman A.P., White T.R., 1988, ApJ 335, 57
Lister M.L., Aller H.D., Aller M.F., et al., 2009, AJ 137, 3718
Longinotti A.L., Cappi M., Nandra K., et al., 2003, A&A 410, 471
Magdziarz P., Zdziarski A.A., 1995, MNRAS 273, 837
Malizia A., Bassani L., Stephen J.B., et al., 2003, ApJ 589, L17
Mannheim K., 1993, A&A 269, 67
Matt G., Porquet D., Bianchi S., et al., 2005, A&A 435, 867
McHardy I.M., Gunn K.F., Uttley P., Goad M.R., 2005, MNRAS 359, 1469
Nilsson K., Pursimo T., Sillanpää A., et al., 2008, A&A 487, L29
Piner B.G., Pant N., Edwards P.G., 2008, ApJ 678, 64
Ponti G., Gallo L.C., Fabian A.C., et al., 2010, MNRAS 406, 2591
Porquet D., Reeves J.N., 2003, A&A 408, 119
Pucella G., Vittorini V., D'Ammando F., et al., 2008, A&A 491, L21
Reeves J.N., Turner M.J.L., Pounds K.A., et al., 2001, A&A 365, L134
Reynolds C.S., 1996, Ph.D. thesis, University of Cambridge
Ross R.R., Fabian A.C., 2007, MNRAS 381, 1697
Seyfert C.K., 1943, ApJ 97, 28
Shu F.H., 1991, The Physics of Astrophysics, Vol. I. Radiation, University Science Books, Mill Valley, CA
Sikora M., Begelman M.C., Rees M.J., 1994, ApJ 421, 153
Soldi S., Türler M., Paltani S., et al., 2008, A&A 486, 411
Tanaka Y., Nandra K., Fabian A.C., et al., 1995, Nat 375, 659
Tavecchio F., Maraschi L., Ghisellini G., 1998, ApJ 509, 608
Türler M., Chernyakova M., Courvoisier T.J.L., et al., 2006, A&A 451, L1
Türler M., Paltani S., Courvoisier T.J.L., et al., 1999, A&AS 134, 89
Turner T.J., Miller L., 2009, Astron. Astrophys. Rev. 17, 47
Urry C.M., Padovani P., 1995, PASP 107, 803
Whitney A.R., Shapiro I.I., Rogers A.E.E., et al., 1971, Science 173, 225
Wilms J., Reynolds C.S., Begelman M.C., et al., 2001, MNRAS 328, L27
Woltjer L., 1959, ApJ 130, 38
Zdziarski A.A., Johnson W.N., Magdziarz P., 1996, MNRAS 283, 193
Zensus J.A., 1997, ARA&A 35, 607